# Single Wall Carbon Nanotube based Nanoparticles and Hydrogel for Cancer Therapy

By

Shuhan Liu

Student Number: 7692183

A Thesis

Submitted to the Faculty of Graduate Studies Partial Fulfillment of the Requirements for the Degree of

**Master of Science**

Department of Textile Science

Faculty of Human Ecology

University of Manitoba

Winnipeg, Manitoba

# Contents

# Chapter 1 Abstract

Nowadays, cancer treatment and tissue regeneration have attracted large amount of attention. Single Wall Carbon Nanotubes (SWNT) possess large surface area and outstanding optical and electrical performance, making it a promising component in cancer therapy and tissue reengineering systems. In this study, four disease treating systems based on SWNT are developed. They are pH-sensitive poly(ethylene glycol)-doxorubicin(PEG-DOX)@SWNT drug release system, temperature sensitive SWNT hydrogel, SWNT based biocompatible magnetic hydrogel and biocompatible SWNT-gelatin-F127-cysteamine hydrogel for tissue engineering. The successfully synthesized target compounds are characterized by FTIR. The *in vitro* release of drugs from the drug release systems is evaluated upon changes of pH values and the laser scanning. The effect of cancer treatment systems on specific kind of cells are examined by confocal laser scanning microscopy (CLSM). The results indicate that all of the four systems show great potential in the biomedical applications especially in disease therapy applications.

# Chapter 2 Introduction

Introduced by Iijima in 1991 [1], carbon nanotubes (CNTs) have been applied in various aspects because of their large surface area, unique optical and electrical property [2, 3]. On one hand, the unique electric and optic properties of CNTs offer the potential to apply them in diagnosis and treatment towards tumors, especially those grow deeply inside the human body, such as hysteroma which is hard to detect and treat even in an early stage by traditional methods, and to apply them in cardiopathy which need specific conductive objects to stimulate heart beats [4, 5]. On the other hand, drugs and biomolecules could be non-covalently or covalently coated onto CNTs to make CNTs a promising drug carrier.

Chemotherapy is a routine clinical approach to treat tumors [6]. Doxorubicin (DOX) is broadly used in cancer therapy and its mechanism is to inhibit bimolecular synthesis by inserting DOX to DNA [7, 8]. Like other cancer drugs, DOX is notorious toxic to human by killing both cancerous and healthy cells [9]. To address these concerns, there is an increasing demand for developing effective drug delivery systems, so that drugs can be delivered to cancerous cells directly and cause minimum damages to healthy cells. Stimuli responsive materials are suitable vehicles to deliver drugs by responding to the chemical-physical environment of tumor tissues. For example, triggered by such external stimuli as light, pH, redox, drug released from the carriers can be greatly enhanced.

Another issue in tumor treatment is that diversity of cancers always evades efficacy of monotherapy.

Light sensitive materials as drug carriers are promising in cancer therapy. Recently, near-infrared radiation (NIR) has become an effective stimulus in drug delivery systems. One benefit of using NIR at 808nm is that NIR can penetrate the skin and underlying tissues with minimum absorbance, as compared to other radiation [10-12]. PH sensitive delivery systems are frequently used in cancer treatment, as the lysosomes in cells of solid tumor are acidic. For example, the pH value in cytosols of normal tissues is 7.4, but it drops from 6 to 5, or even lower in early endosomes, late endosomes and lysosomes [13]. Because of the exuberant production of lactic acid, the extracellular area of most tumors is mildly acidic [14, 15]. Many methods have been conducted to endow mateirals pH sensitive, such as using hydrazone bonds, Schiff base and titratable amine groups in polymers.

Thermo-sensitive hydrogels based on CNTs is also very promising in the area of cancer treatment. Hydrogels are cross-linked hydrophilic polymers which are insoluble and can swell in aqueous solutions [16]. Because of the large amount of water contained in the hydrogel networks, which is similar to that in the tissues of the human bodies, hydrogels usually exhibit outstanding biocompatibility. Thermo-sensitive hydrogels based on CNTs can combine the advantages of both hydrogels and CNTs and show promising potentials in the field of cancer treatment. Many achievements have been obtained in the application of CNTs in biomedical areas [17-21]. Still, more efforts are needed to further enhance their functions.

Superparamagnetic iron oxide is magnetic and biocompatible, making it prospective in biomedical areas [22, 23]. Magnetic nanoparticles composed of $Fe_3O_4$ have been be used for many purposes, such as biosensors, bioseparators, vehicles to delivery drug and contrast agents applied in magnetic resonance imaging (MRI)[24, 25]. SWNT based Magnetic hydrogels integrate the outstanding properties of carbon nanotube and magnetic nanoparticles, therefore, can be used as scaffolds for cell growth and can further be applied in cardiac tissue engineering.

Aggregation of CNT in cells can lead to cellular immune responses. Surfactant are therefore needed to achieve well dispersed CNT solutions [26]. Triton X-100 and Tween 80 have been used as dispersant for CNT, but in-vitro cell tests showed that both of them are toxic[27]. F-127 has been found to be a good surfactant that disperses SWNT uniformly and stably. The F-127 is also considered to be low toxic [28, 29]. The combination of CNT and F-127 exhibits promising potential in biomedical applications.

In this thesis, four tumor therapy systems based on SWNT are developed. The first is NIR-pH dual sensitive functional single-wall carbon nanotubes for cancer therapy. The results suggest that PEG-DOX@SWNT micelles are pH sensitive, and the drug release from PEG-DOX@SWNT micelles can be triggered by the irradiation of NIR and/or change of pH values. The second is a temperature sensitive single wall carbon nanotube hydrogel. The results indicat that the inhibition effect of this thermo-sensitive hydrogel towards cancer cells can be obtained after exposure to NIR. The third one is silica coated magnetic nanoparticles for cancer treatment. The results show that the silica-coated Fe3O4 nanoparticles can provide good support for stem cell growth. The fourth one is a biocompatible SWNT-Gelatin-F127-cysteamine hydrogel for tissue engineering. The results reveal that SWNT based Gelatin-F-127-cysteamine hydrogel have good compatibility for ADSC and the SWNT in which is very stable and well distributed.

# Chapter 3 Literature Review

With the development of nanotechnology, nanomaterials have found more and more applications in the biomedical field. Compare to the traditional methods of oral administration or injection, utilizing nanoparticles to delivering drug into the human body is more effective and precise: after entering into the human bodies, these drug-loaded nanoparticles may automatically target and attack cancerous cells or repair damaged tissue [30-32]. Owing to their special structures and properties, carbon nanotubes have been widely applied in biomedical fields. Recently, their huge potential of being drug carriers in the early diagnosis and treatment of tumours has drawn lots of attentions.

Extensive research has focused on either using non-covalently functionalized SWNT as a DOX carrier, or modifying DOX with PEG to produce a pH-sensitive polymer. Both approaches improve the efficiency of drug delivery. However, there has been little research on combining SWNTS, PEG-DOX, and NIR. It is therefore desirable to develop an improved drug delivery system based on this method. Moreover, many studies have shown that hydrogel and gelatine have good biocompatibility and SWNT has unique NIR absorbing ability. Thus it is desirable to exploit an improved thermo-sensitive hydrogel based on SWNT.

## 3.1 Drug Delivery Systems

The side-effects of drugs are receiving more and more concerns in recent years. To a huge extent, the side-effects may be caused by inappropriate methods in which drugs are put into human bodies.

When the commonly used intermittent input method is conducted, to ensure that the minimum required concentration of drugs inside bodies could maintain, over dose is inevitable, which may damage the healthy cells or tissues. Therefore, it is essential to build a drug delivery system that directly targets the cancerous cells or tumors. Through selecting a proper drug delivery route, drug delivery systems may offer accurate dose, safely and efficient treatment. Targeted drug delivery system directly targets drugs to the lesions with little damage to the surrounding normal organs, tissues and cells, therefore enhances the effectiveness and decreases the side-effects [33]. A drug delivery system consists the drug and the drug carrier. Drug carrier plays a significant role in the system.

An effective method to make bioactive molecules degraded by organisms is to use nanomaterials (nanoparticles, nanorods, nanotubes or nanowires) to wrap bioactive molecules and to deliver them into the organisms. Carbon nanotubes (CNTs) are one type of these nanomaterials. Carbon nanotubes have many fascinating physicochemical properties [3, 34], such as high conductivity, high mechanical property and low weight. The surface of CNTs can be functionalized. The functionalized surface can be either the inner or outer wall of the hollow tube.

The inside hollow part of CNTs can contain large amount of drugs. Once opened, the opening end of the CNTs allows drug to be released [35]. The more vital part is that CNTs can separate the loaded drugs from the environment, therefore prevent the potential drug loss in the process of drug delivery, including drug degradation by the physiological environment or the drug aggregation caused by electrostatic effect, thereby, drugs can be safely transported into cells. Nowadays, owing to the special advantages of CNTs, they have drawn lots of attention from global scientists as a new kind of promising drug vehicles applied in the anti-cancer drug delivery systems [36].

## 3.2 CNTs

CNTs, as a type of one dimensional nanomaterials, have low weight, perfectly connected hexagonal structure and many exceptional mechanical, electronical, and chemical properties [2, 34]. Extensive research on CNTs and nanomaterials have been conducted over the recent years. The prospective applications of CNTs have continuously emerged at the same time.

### 3.2.1 Physicochemical Properties of CNTs

CNTs have a typical lamellar hallow structure. Their radial dimension is at the nanometer level, while their axial dimension is at the micrometer level, and the two ends of the tubes are usually closed. The distance between the layers that form carbon nanotubes is about 0.34nm, and certain intersection angle exists between those layers. The diameter of CNTs generally ranges from 2 nanometers to 20 nanometers[37] . The tubular parts of CNTs usually have a pentagonal cross section. The tubes themselves are composed of hexagonal carbon micro construction unit, the ending caps of CNTs have a polygon structure (or known as a multilateral tapered multi-wall structure) composed of pentagonal carbon atomic rings. CNTs have found their potential applications in many different fields.

Based on the number of graphite sheets, CNTs can be divided into two types: Single-walled nanotubes (SWNTs) and Multi-walled nanotubes, (MWNTs)[38]. During the formation of MWNTs, the middle layers of graphite sheets may easily become a trap centre and capture a variety of defects. Therefore the walls of MWNTs are usually covered with small hole-like defects. Compared with MWNTs, SWNTs are composed of a single layer of graphite, and the

diameter of SWNTs only varies within a narrow range. Consequently they haveless defects and higher uniformity.

CNTs can also be categorized into three types based on their structural feature; they are carbon nanohorns, nanobuds and nanotorus. The length of CNTs can be cut via physical or chemical methods, allowing them to enter into cells more easily and making them more suitable for drug carriers [39]. In addition, the ends of CNTs can be opened and offer more room to load drugs. The side walls of CNTs can be chemically functionalized so as to make it easier to carry drugs.

### 3.2.2 CNTs in imaging

CNTs have unique physicochemical properties. For example, they can absorb infrared light and their temperature are increased as a result, making them possible to be applied in deep tissue heat treatment[40]. They can also emit infrared fluorescent and be applied in the internal imaging diagnose.

It has been reported that a non-destructive imaging of SWNTs' distribution inside live drosophila can be observed, owing to the particular near infrared fluorescent emitted by SWNTs. Pasty fermentation power with different dose of SWNTs were used to feed just hatched drosophila larvae. After the first feeding stage (4-5days), the weights of larvae were increased by 200 times. They then turned to pupae, finally grew into imagos. The following results were obtained after observing the drosophila's progress of growth and the images of SWNTs in vivo[41]:

1. The SWNTs ate as food by drosophila larvae will not affect their growth, and major physiological function such as their reproductive capacity after they become adults. Also the addition of SWNTs with different dose did not cause any short term toxicity.

2. The SWNTs spread in drosophila can be observed through the near infrared fluorescent emitted by them, destructive operations (for example: tissue slice) are not required.

3. Only a very small amount of SWNTs were absorbed into tissues, the majority of SWNTs in-taken by drosophila were finally ejected through their digestive system, and no harmful effect was brought to drosophila.

The research has shown the potential of SWNTs' application in nanomedicine. Firstly, the unique property of SWNTs to emit near infrared fluorescent allows the distribution of SWNTs be non-destructively observed in vivo, offering promising internal diagnose methods; Secondly, SWNTs do not bring any obviously harmful effect in living organism, thus show great potential to act as drug delivery cargos in vivo[41].

## 3.3 CNTs as Drug Delivery System

A nanomaterial, CNTs can load biologically specific molecules and drugs and transport them into cells or tissues. The cell penetrating properties of biological macromolecules (protein and nucleic acid) and some drugs are poor. In order to transport them into cells, they can be adsorbed or coupled into the carriers, like CNTs, that can penetrate cell membrane [42]. In addition, because of the strong π-π interactions, the biomolecules or drugs that contain amino groups can be attached to the surface of CNTs. Owing to the large surface area and excellent membrane penetration property of CNTs, they have drawn lots of attention in the field of drug delivery.

### 3.3.1 The cell membrane penetration property of CNTs

One of the vital characteristics of CNTs is that they can cross cell membranes and various barriers inside organism and enter into cells and many kinds of internalorgans [43-46]. Research show that CNTs can pass through membranes of a variety of cells, including fibroblasts of mouse, cervical cancerous cells, breast cancerous cells, T-cell and lymphoma cells of human beings and Jurkat cells.

Owing to the cell membrane penetration property of CNTs, they can be used as drug vehicles and transport biomacromolecules into cells. Pantarotto et. al. used isothiocyanato fluorescein to mark the derivative-modified SWNTs and peptide-coupled SWNTs and investigated their cell membrane penetration capabilities. It was found that both of them can cross cell membranes: derivative-modified SWNTs mostly enter the cytoplasm while the peptide-coupled SWNTs access nucleus [46].

Shi Kam et. al. used strep tavidin to modify SWNTs and imported them into human promyelocytic leukemia cells and T-cells. They found that the modified SWNTs can enter cell lines with both sticky and non-sticky walls. Cells did not uptake loose fluorescent strep tavidin but they did uptake strep tavidin-modified SWNTs. The mechanism of SWNTs' entering into cells was believed to be cell endocytosis [47].

### 3.3.2 Drug coating of CNTs

When used as drug carriers, CNTs can be coated with drugs via three approaches: absorption, covalent grafting, and non-covalent grafting. Take advantage of the high surface area of CNTs, the approach of absorption is usually achieved by mixing modified CNTs with drugs in a solvent for hours or days until the solvent evaporates [48-50] . Composites obtained by this method usually

have a rapid release spike at the very beginning of drug release profile, because a major portion of drugs are absorbed only on the surface of the CNTs. After the spike, drug release becomes stable, due to the fact that the rest of the drugs are controlled by Van der Waals force and hydrogen bonds.

### 3.3.3 CNTs as drug carriers

Ajima et. al. used oxidated SWNTs as cargos to carry cis-platinum. Cis-platinum was embedded inside the tube of SWNTs, and was slowly released into the phosphate buffer and cell culture medium to prevent the growth of human lung cancerous cells. However, the cis-platinum was not released if pristine SWNTs were used, indicating that the chemical modification can improve some properties of SWNTs and make them more suitable for drug carrier[48].

Murakami et. al. utilized both pristine SWNTs and oxidated SWNTs as vehicles to transport hexadecadrol. They discovered that compared with pristine SWNTs, oxidated SWNTs show better compatibility towards hexadecadrol, indicating that modifications can enhance the compatibility. In phosphate buffer solution(pH 7.4), hexadecadrol was slowly released and no obvious toxicity was observed [49].

## 3.4 The functionalized modification of CNTs

CNTs are not soluble in organic solvent and water, which impedes their applications in the area of drug carriers. The functionalization of CNTs can improve the solubility as well as the biocompatibility of CNTs [4]. These modifications make CNTs more appropriate in drug delivery field.

Foldvari et al. proposed several methods to make CNTs distribute in soluble[51]: the addition of surfactants, the functionalization of CNT side-walls, the utilization of biomolecules. Among them, functionalization is the most effective method[51] .

The most frequently utilized modification in recent years is chemical functionalization, either to covalently bind chemical molecules to the surface of CNTs (covalent functionalization), or to have functionalized molecules absorbed/coated onto the surface of CNTs (non-covalent functionalization).

### 3.4.1 Covalent Functionalization

Secure fixation of functional molecules onto CNTs can be obtained by covalent bonding. Hydrophilic groups, like COOH and OH, can be added to CNTs after oxidization, and further react with SOCl and carbodiimide. Functional composites that are capable of reacting with other mixtures are obtained as a result [51, 52].

Carboxylic acid groups can also be added to the open ends of CNTs or defects caused by strong acid treatment. CNTs as drug carriers may have different lengths and electronic properties, which can be achieved by applying strong acid treatment. The degree of defection can be controlled by cutting CNTs into shorter ones.

Drugs with low water-solubility can be covalently conjugated on CNTs to increase their solubility, reduce their toxicity that could have been caused by aggregation of drug molecules, and enhance their delivery efficiency.

Covalent functionalization of CNTs may change the structures of CNTs permanently. However, reactive species such as arynes, carbenes, or halogens are often required for the reactions, and it is

hard to accurately control the reaction sites and adding methods [53]. Furthermore, the reactions to form covalent bonds usually occur in extreme conditions.

### 3.4.2 Non-covalent Functionalization

The surface of CNTs can be non-covalently functionalized with polymers, polynuclear aromatic compounds, surfactants, and bioactive molecules, to enhance their dispersity. Such non-covalent functionalization is based on π-π interactions, Van der Waals forces and hydrophobic interactions so it does not modify the electronic properties of CNTs [17, 54-56].

Non-covalent functionalization is performed by mixing drugs or bioactive molecules with CNTs followed by ultrasonic dispersing. This method can attach drug molecules on CNTs surfaces while dispersing CNTs at the same time. The disadvantage is that the balance of solution can be easily broken, causing detachment of absorbed drugs and precipitation of CNTs.

## 3.5 Biosafety of SWNTs as Drug Carriers

Before using CNTs as drug carriers in clinic, their biosafety should be fully investigated. Many studies suggest that CNTs are safe, while other studies have reported tissue damages in vivo and cell damages in vitro.

Cheng et al. investigated the effects of FITC-labeled PEGylated single-wall CNTs (FITC-PEG-SWNTs) in living cells. PEGylated single-wall CNTs were observed inside of cell nuclei, with no abnormal changes in the nucleus structure, growth kinetics and cell cycle distribution [57].

Magrez et al. performed in vitro tests to study the cytotoxicity of MWNTs, nanofibers, and nanoparticles in lung cancer cells. They found that all samples have certain level of cytotoxicity, which is closely related to their sizes, and MWNTs have the lowest cytotoxicity among the three [58].

Murugesan et al. discovered that the cytocompatibility of CNTs can be improved by increasing their solubility and coupling them with bioactive molecules. Heparin modified MWNTs were shown to have good cytocompatibility in the in vivo tests [59].

Although the biosafety aspect of CNTs as drug carriers has not been fully understood, we do know that their cytotoxicity is related to their sizes, which means it is possible to minimize toxicity by controlling the size while fabricating CNTs. Modifying the surface of CNTs with bioactive molecules can also reduce their toxicity. All these make CNT a promising choice for drug carriers.

## 3.6 Doxorubicin

Doxorubicin (DOX) is an anthracycline antibiotic that functions as a DNA intercalating agent. It is effective against various kinds of cancers by inhibiting macromolecular biosynthesis. DOX is usually administered intravenously, and its efficiency is really low due to the fact that it is inefficiently distributed, poorly selective, and unable to penetrate into cells. More over, DOX is very toxic in human body and can bring many side-effects.

Carbon nanotubes (CNTs) have large surface areas and hollow spaces, therefore can be used to immobilize DOX and become an anticancer drug delivery systemto transport DOX through cellular barriers.

Park et al. explored the possibility of using poly-1-coated CNTs as drug carriers for DOX. The

aromatic rings in DOX can react with CNTs' surface by π-π stacking, and the positively-charged amine groups in DOX can react with carboxylic acid residues in the polymers. Drug release tests showed high drug loading efficiency, and XTT assay showed enhanced cytotoxicity against B16F10 melanoma cells [60].

Heister et al. used triple functionalization of oxidised SWNTs as the carriers for DOX. Using carcinoembryonic antigen (CEA) as a fluorescent marker, the authors monitored the cellular uptake process of DOX under confocal microscopy. Results showed that SWNTs and DOX successfully entered the WiDr colon cancer cells, and DOX was found inside cell nuclei while SWNTs stayed in cell plasma [61].

Zhang et al. used functionalized SWNTs as nanocarriers and developed a new drug release system. This system consists of polysaccharides(ALG and CHI)-functionalized CNT as drug carriers, folic acid as the targeting part, and DOX as the anticancer drug. It was shown that the new drug release system had high release rate in low pH environments corresponding to typical tumor tissues. DOX with the CNT carriers was found to get into cell nuclei with higher efficiency and lower side-effects as compared to the free DOX control samples [44].

Liu et al. used π-π stacking to load DOX on polyethylene glycol-functionalized SWNTs. In vivo trials revealed that this drug release system treated a larger percentage of tumors than the free DOX and DOXIL, and side-effects were also significantly lower [62].

Ali-Boucetta et al. developed another drug release system based on π-π stacking, and composed of a DOX-MWNT non-covalent composite. MTT assay was performed on MCF-7 cells. Enhanced cytotoxicity was observed in DOX-MWNT as compared to free DOX and DOX–pluronic composite [63].

Li et al. firstly oxidized multi-wall carbon nanotubes, then synthesised folate and iron di-functionalized multi-wall carbon nanotubes (FAMWCNT@Fe). After loading DOX on the FAMWCNT@Fe, the composite was released into HeLa cells under magnetic field. Results showed higher drug loading efficiency and extended drug release duration. Drug delivery tests were also performed, indicating a six-fold improvement in delivery efficiency over free DOX[64] .

Chen et al. modified multi-wall carbon nanotubes in nitric acid to obtain carboxylated multi-wall carbon nanotubes (c-MWNTs), and then used π-π stacking to fabricate a composite composed of epirubicin hydrochloride (EPI), an analog of DOX, and c-MWNTs. Results showed significant improvement in load efficiency compared to MWNTS, and that the load efficiency is inversely proportional to the diameter of c-MWNTs [65].

All the above research show that DOX-loaded functionalized CNTs can be fabricated into a new drug release system using π-π stacking. Such a new system has excellent drug loading efficiency and drug release behavior. Cytotoxicity is also enhanced against cancerous cells. None of the research, however, focused on the controlling aspects of drug release, which demands smart drug carriers that reacts to the environment and release drugs on targeting sites.

## 3.7 Stimuli-responsive Nanocarriers

It is desirable to make polymeric nanoparticles stimuli-responsive, or “smart”, when used as drug carriers. Once the nanocarriers become active participants instead of passive vehicles, they have the potentials to greatly increase delivery efficiency as well as to reduce the side effects [66].

Stimuli-responsive nanocarriers undergo changes in their physical or chemical properties when exposed to stimuli, including both physical and chemical stimuli. Common physical stimuli include

temperature, electrical field, magnetic field, light, and ultrasound, while common chemical stimuli include pH, ionic strength, enzyme, and chemicals. Stimuli-responsive nanocarriers are especially effective against diseases with unique stimuli, so that the nanocarriers can respond specifically to the "triggers".

### 3.7.1 pH-responsive Polymer-drug Conjugates

pH sensitive nanoparticles have drawn lots of attention recently due to the fact that pH values differ in various human tissues. For example, the pH value of most normal human tissues is around 7.23, while tumor tissues have a significant lower pH value of 6.75 [67-70].

One of the important applications of pH sensitive nanoparticles is drug delivery. Acid sensitive spacers are commonly used to connect the drug and polymer, so that drug release would be triggered either in relatively acidic extracellular fluids or, after endocytosis in endosomes or lysosomes of tumor cells.

Kataoka et al. synthesized a series of pH sensitive nanoparticles by conjugating DOXto pH sensitive polymeric carrier PEG-b-PAsp [71]. The bond between DOX and PEG-b-PAsp breaks rapidly in weak acidic environment, causing the release process of DOX. DOX is a widely used anti-cancer drug, and the hydrophobicity of DOX enables the self-assembling process of nanoparticles. It was revealed that the conjugate is very stable under the physiological pH (7.4), while rapid drug release was observed in acidic environment corresponding to endosomes or lysosomes (pH 5 – 6). Further studies indicate that, with the aid of TβR-I receptor, this nanoparticles carrier is highly effective

against many troublesome cancers including pancreatic cancer and hereditary diffuse gastric cancer[71].

Bae et al. created many pH sensitive polymeric nanoparticles using sulfonamide and histidine, and such nanoparticles are capable of controlled drugs release in a relative narrow pH range (6.5 – 7.2) [72-74].

## 3.8 Hydrogels

Hydrogels are cross-linked hydrophilic polymers which are insoluble but can swell in an aqueous solution. Hydrogels can also be defined as a tridimensional cross-linked polymer network with porous structure that is capable of preserving large amount of water [16]. The existence of hydrophilic regiments (carboxyl, hydroxyl amino groups) in the polymer can lead to the enhancement of water preserving ability.

Hydrogels can be sorted in lots of methods. In a general way, the polymerized gels are either inartificial (collagens) or composited. Moreover the hydrogels can be classified into two kinds based on their cross-linking characteristics. The hydrogels are known as perpetual ones if the covalent bonds form during the cross-linking reaction. On the other hand, the hydrogels are classified as physical ones if the formation of hydrogels is caused by physical reactions, for instance: ionic interaction, van der Waals force, hydrogen bonds [75-77].

Hydrogels can also be sorted into conventional and irritation sensitive hydrogels[78]. Conventional hydrogels absorb water with no variation inof equilibrium swelling upon the alternation of pH, temperature or other stimulations form exterior environment. The irritation sensitive hydrogels can

quickly vary their equilibrium swelling upon the alternation of environmental conditions. The irritation sensitive hydrogels can be further classified into many classes depending on the irritation types, such as light-sensitive, thermo-sensitive, electro-sensitive, pH sensitive, etc.[79-81].

Thermo-sensitive hydrogels are usually characterized by the existence of hydrophilic groups (ethyl, methyl). PNIPAM is one of the most popular thermo-sensitive polymers. PNIPAM is characterized by a relatively low critical solution temperature, about 32°C in water, above which the hydrogels transform from swelling form into de-swelling form [82].

## 3.9 Magnetic nanoparticles

Magnetic nanoparticles are formed by Fe2O3, Fe3O4. There are lots of chemical ways for magnetic nanoparticles synthesis. Coating is a very essential step after synthesizing nanoparticles, because this procedure can prevent the aggregation instability of nanoparticles. Coated magnetic nanoparticles can dissolve in biologic liquids or water solutions[83].

Various kinds of polymers can be chosen for coating materials, for instance, (3-Aminopropyl)trimethoxysilane (APTS), carboxymethylated dextran, PEG, starch, organic siloxan, glycosaminoglycan[84]. APTS is an outstanding option among these polymers and has been widely utilized to form the coating layer outside the magnetic nanoparticles.

The magnetic nanoparticles can be used in a lot of biomedical applications, such as magnetic target therapy and magnetic hyperthermia. Moreover, they show very promising potential in the application of cardiopathy treatment owing to their electrical conductivity.

# Chapter 4 NIR-pH Dual Sensitive Functional Single-wall Carbon Nanotubes for Cancer Therapy*[85]

## 4.1 Materials and Methods

### 4.1.1 Materials

All chemicals were purchased from Aldrich Chemical Co. (St. Louis, MO, US) and used without further purification unless otherwise mentioned. Methoxy poly (ethylene glycol) - succinimidyl (5K) (PEG-SCM) were purchased from JenKem Technology USA Inc. (Allen, TX, US). Dialysis membrane (cut-off=7 kDa MWCO). Pristine single-walled carbon nanotubes (Timesnano, prepared by chemical vapor deposition method, 90 wt % pure SWNTs, 1-2 nm in diameter and several micrometers in length) were used without further purification. MCF-7 cells were gifted from Dr. A Raouf (Manitoba Cancer Care).

---

* Reproduced from [85] with permission from The Royal Society of Chemistry.

## 4.1.2 Synthesis of DOX-PEG Conjugates via Hydrazone Bonds

### 4.1.2.1 Synthesis of PEG-hydrazine

The typical synthesis of PEG-hydrazine was described as below: 600 mg of Methoxy PEG(5K) succinimidyl carboxymethyl ester and 160 mg of hydrazine were dissolved in 10 ml phosphate buffer solution (PBS) buffer solution (pH=7.4) and stirred for 24 hours. The product was then dialyzed against distilled water for 2 days to remove the excess hydrazine molecules. The final product was obtained by lyophilization and rate of yield was 90 %.

### 4.1.2.2 Synthesis of PEG-hydrazone-DOX

The synthesis of PEG-hydrazone-DOX was recorded the reference with modification [86, 87]. Briefly, 500mg of PEG-hydrazine and 50mg of DOX were dissolved in 10 ml of anhydrous DMSO and stirred for 3 days at dark in room temperature. The product was then purified by precipitation in largely excess of diethyl ether for two times. The red powder was dried in high vacuum for 24 hours and the rate of yield was 90 %.

The chemical structure was next characterized by $^{1}$H NMR analysis. $^{1}$H-NMR spectra were recorded using a Bruker Avance 300 NMR spectrometer (300 MHz) with d6-DMSO as the solvent.

## 4.1.3 Preparation of Oxidized SWNTs

The oxidized SWNTs was prepared according to a previous research with modification[88]. Briefly, 50 mg of SWNTs was added into the solution mixed by 98 % $H_2SO_4$ and 65 % $HNO_3$ with volume

ratio of 3 to 1, and then the mixture was sonicated at 0 °C for 24 hours. Next, the oxidized SWNTS was washed by ultrapure water (18.2 MΩ) for five times and filtered by micro-porous filtration membrane (0.2 μm). The oxidized SWNTs were collected by centrifuge and then dried in high vacuum for 24 hours. The hydrodynamic diameter and size distribution of oxidized SWNTs were measured by dynamic light scattering (DLS). Measurements were conducted at 20 °C utilizing Brookhaven ZetaPals. Solution of oxidized SWNTs (0.1 mg/mL) was passed through a 0.45 μm pore size filter in advance. The XPS analysis was performed on an Axis Ultra DLD X-ray Photoelectron Spectrometer. Base pressures of the Al Ka (1486.6eV) monochromatic source was less than 10-8 Torr and the spectra of the sample was determined at a fixed take-off angle of 45°. A hybrid lens mode was utilized at a pass energy of 20eV for the high resolution scanning. High resolution scanning was employed for C 1s. C 1s with a binding energy of 284.6eV was applied to correct the energy shift caused by surface charging. Background subtraction was conducted by CasaXPS® software, peaks were then fitted (Gaussian/Lorentzian curves).

### 4.1.4 Preparation of PEG-DOX@SWNTs nanoparticles

Through π-π stacking interactions, electrostatic interaction, hydrophobic interactions, doxorubicin (DOX) could be bound to CNTs non-covalently [44, 54, 89, 90].

SWNTs were coated with PEG-DOX according to the previous research [91]. To disperse SWNTs in PEG-DOX aqueous solution, 20 mg of PEG-DOX copolymer and 4 mg of SWNTs were added into a 10 mL vial with 3 ml DMSO, and the mixture was sonicated for 60 minutes, the solution was then stirred in the dark for 24 hours. The homogeneously black solution was obtained. The black

solution was then added into a dialysis bag (MWCO = 7000 Da) and dialyzed against Milli-Q water for 3 days to remove the excess amount of unbounded DOX molecules and DMSO. The PEG-DOX@SWNTs nanoparticles were then obtained by lyophilization and stored in -20 $^{0}$C for further use. By utilizing UV–vis spectroscopy, the drug-loading efficiency of DOX loaded nanoparticles in DMSO was quantified by referring to its absorbance at 480 nm. The drug loading efficiency was calculated based on the following equations:

Drug loading efficiency = (weight of loaded drug/weight of feeding drug) × 100%

The hydrodynamic diameter and size distribution of PEG-DOX@SWNTs nanoparticles were explored by DLS, the Measurements were conducted at 20 °C using Zetasizer Nano-S from Malvern Instruments. Solution of the PEG-DOX@SWNTs nanoparticles (0.1 mg/mL) was passed through a 0.45 μm pore size filter previously.

### 4.1.5 Determination of PEG-DOX@SWNTs nanoparticles

Fourier transform infrared spectroscopy (FTIR) test was adopted applying an IR Spectrophotometer (Bruker IFS 66v/s, German) within limits between 4000–400 cm$^{-1}$. $^{1}$H NMR measurements were examined on a Bruker (500 MHz) NMR instrument. The morphology of PEG-DOX@SWNTs nanoparticles were determined by a Joel 1010 Transmission Electron Microscope (TEM), setting accelerating voltage at 80 KV, employing a LaB6 filament and equipped with an AMT digital camera. Micrographs were acquired at 60,000× magnification. Also, the DOX fluorescence

distribution of PEG-DOX attached into SWNTs was investigated by multimodal nonlinear optical imaging microscopy (NLOM).

### 4.1.6 pH-dependent in vitro doxorubicin release from the PEG-DOX@SWNT.

In this study, drug release behavior from the PEG-DOX@SWNT was explored. Four groups of samples were prepared in the release profile named as a, b, c and d, and the concentration of DOX kept same as 0.2 mg/ml in all samples. Sample a and b were treated by laser irradiation, they are prepared by following method: Two 20ml class bottle contained 2 ml 2.67 mg/ml SWNT/DOX-PEG (the concentration of DOX is 0.2mg/ml) solution was treated by NIR laser with wavelength of 800nm and the power of 900 mW for 5 minutes. Sample c and d were not treated by laser. Then, four groups of samples were added into dialysis bag (MWCO = 7000 Da). The bags were sealed and put into 10 ml of PBS with different pH with stirring at 85 rpm at 37℃ in dark. The dialysis bags hold sample a and c were submerged in to PBS with pH 5.0, the other two dialysis bags were submerged into PBS with pH 7.4. 5 ml incubation solution was taken out from 10 ml incubation solution at preconcerted intervals; 5 ml fresh buffer solution was then added to remain the incubation volume at 10 ml. The solutions taken out were tested by UV-vis spectrometry at 490 nm, which is the characteristic maximum absorbance of DOX in solution. All of the release tests were employed for three times.

### 4.1.7 Cell uptake and intracellular drug distribution of PEG-DOX@SWNTs

Confocal laser scanning microscopy (CLSM) was applied to investigate the cellular uptake and drug distribution of DOX by incubating the MCF-7 breast cancer cells with released PEG-DOX@SWNT in Acetate buffer at pH 6.0 (0.1 M) and PBS buffer at pH 7.4 (0.1 M) at release time points of 15 minutes, 2 hours and 24 hours respectively. Firstly, the MCF-7 cells were incubated in the culture dish which was covered by glass slip at a density of 2 x $10^5$ cells/dish (diameter = 3.5 cm) and cultured for 24 hours. Next the cells were incubated with samples in different incubation pH. PBS buffer was then used to wash cells for three times after preconcerted incubation time. 4 % paraformaldehyde PBS solution was added to fix cells, then wash the cover slip with PBS buffer for three times after 15 minutes of incubation. The permeabilization was accomplished by addition of 0.1 % Triton X-100 PBS buffer then incubate for 10 minutes followed by rinsing with PBS buffer for three times. the F-actin of the cells were dyed by 10 nM phallacidin/1 % (w/v) BSA solution for 20 minutes to make cell skeleton visible, and then rinsed with PBS buffer for three times. The visualization of the cells nuclei was accomplished by incubation in 10 nM Topro-3 for 20 minutes and then rinsed with PBS buffer for three times. At last, the cover slip was fixed on a microscope slide and observed by CLSM.

Transmission electron microscopy (TEM) was also applied to determine the intracellular distribution of PEG-DOX@SWNTs. The process of TEM used to observe cells was described previously[92]. After 2 hours of incubation with MCF-7 cells, cells were washed with PBS three times to remove nanotubes in medium. Then cells were fixed in a solution consisting of 2.5% gluteraldehyde in 0.1M Sorensen's buffer for 1 hour. Then the samples were washed with 5% sucrose solution in 0.1M

Sorensen's buffer for 5 minutes 3 times and put into fridge at 4°C overnight. Post-fixation was processed by adding 1% OsO4 to the cell samples for 2 hour. After the dehydration with graded alcohols and methanol, samples were embedded in epoxy resin. Followed by dried in an oven at 60°C for 24 hours, thin sections were cut with a microtome (Reichert Nr. 318423, Austria) and mounted on copper grids. Finally, 2% uranyl acetate and 1% lead citrate were used to stain the samples. These prepared grids were analyzed with a TEM (Philips CM-10) at 25°C.

### 4.1.8 Multimodal nonlinear optical imaging microscopy (NLOM)

To study the intracellular location of the nanoparticles in live cells, multimodal nonlinear optical imaging microscopy (NLOM) was applied to achieve in vitro coherent anti-Stokes Raman (CARS) and two-photon excited fluorescence (TPEF) images of MCF-7 cells with nanoparticles. CARS provided label-free visualization of MCF-7 cell structures with sub-micron resolution. PEG-DOX@SWNTS nanoparticles were tracked by intrinsic DOX TPEF signals and SWNTS were tracked by intrinsic SWNTS TPEF signals. The excitation wavelengths used in NLOM are the 800nm near-infrared.

All of NLOM images shown in this paper represent a typical 2 ~ 3 μm depth of view through employing a 40x 0.8 NA objective lens, which is because both CARS and TPEF signals were only created at the focal point of the probing laser beam. A water immersion objective lens (Olympus, 40x 0.8NA WI) which was submerged into culture medium without fixation was applied to obtain the images for live cells in culture plates immediately. CARS microscopy is a strong imaging modality for fast visualization of intracellular and extracellular structures with dense C-H bonds

such as proteins in nucleus, intracellular lipids droplets, cell membrane and extracellular lipid-laden structures in tissue[93]. In this research, the live cells structures and the PEG-DOX@SWNT nanoparticles endocytosed by cells were visualized by CARS. TPEF was particularly employed to image elastin protein and many labeled reporting dyes including DOX.

### 4.1.9 Cell viability assay of released drugs

In order to verify NIR can initiate the pro-drug release from SWNTs. A 20 ml class vial contained 2 ml 1.33mg/ml SWNT/DOX-PEG solution was treated by NIR laser with power of 900 mW for 5 minutes. The cytotoxicity of the released prodrug from PEG-DOX@SWNTS with or without laser treatment was investigated applying a methylthiazoltetrazolium bromide (MTT) assay. MCF-7 breast cancer cells were cultured with Dulbecco's Modified Eagle's Medium (DMEM, GIBCO) added with 10% fetal bovine serum (FBS, GIBCO), 1.0×105 U/l penicillin (Sigma) and 100 mg/l streptomycin (Sigma) at 37 °C in 5 % CO2. The culture density is 8,000 cells per well. After 24 hours of incubation, the medium was removed and different amount of SWNT/DOX-PEG solution (1ul, 2ul, 5ul, 10ul, 20ul, 50ul, 100ul) was mixed with culture medium (99ul, 98ul, 95ul, 90ul, 80ul, 50ul, 0ul) then added to wells and concentration of DOX could reach to 1ug/ml 2ug/ml, 5ug/ml, 10 ug/ml, 20 ug/ml, 50 ug/ml, 100 ug/ml respectively. 10 μL MTT solutions were added to each well after 24 hours of incubation, and cells will be then incubated for 4 h. The medium was then removed followed by adding 200 μL DMSO. The absorbance of each well was determined by a 96-well plate reader at wavelength of 570 nm and 630 nm. The cell inhibition of samples was obtained by the following method:

$$\text{Cell Inhibition Rate} = (I_{control} - I_{sample}) / I_{control} \times 100\ \%$$

$I_{sample}$ represent the intensity of cells with different treatment, $I_{control}$ represent the intensity of untreated cells.

## 4.2 Results and Discussion

### 4.2.1 The characterization of PEG-DOX@SWNT

The hydrazones linkage was achieved by condensating the ketone of DOX with a hydrazine linkage [94-96] [97, 98]. pH sensitive conjugation of PEG-hydrazone-DOX was synthesized through formation of hydrazone bonds between the hydrazine groups of PEG-hydrazine and the ketone group from doxorubicin. The synthetic route was indicated in Fig. 1.

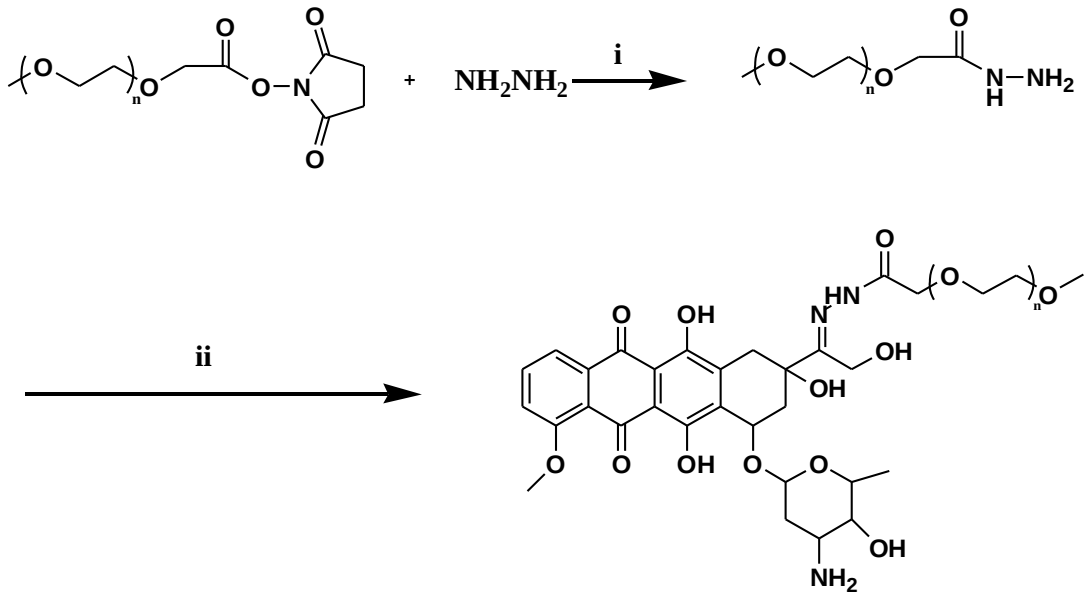


Figure 1 The schematic illustration of synthesis routine of PEG-DOX conjugate with acid sensitive hydrazone bonds. (i) phosphate buffer solution, pH = 7.4, room temperature, 1 day; (ii) doxorubicin, DMSO, room temperature, 3 days.

The chemical structure of PEG-DOX was characterized by $^{1}H$ NMR analysis and FTIR spectrum. As shown in Figure 2, the peaks at 1.19 ppm resulted from methyl group in the conjugated doxorubicin and the peaks at 7.7~7.9 ppm resulted from aryl groups in the conjugated doxorubicin. At the same time, the peaks at 4.19 ppm resulted from methylene groups which is next to the ester group in the conjugated PEG, the peaks at 3.54 ppm resulted from methylene groups in the backbone of conjugated PEG. Based on integral of the peak of methylene protons from conjugated PEG and methyl protons from conjugated doxorubicin, the conjugation yield ratio are that every 100 PEG molecules were conjugated with about 94 doxorubicin molecules.

FT-IR spectroscopy was employed for the characterization of SWNTs, DOX, PEG-CO-NHS, PEG-DOX, and PEG-DOX@SWNT to examine the immobilization of PEG-hydrazone-DOX on SWNTs (Fig. 3). According to previous research, the typical peak of oxidized SWNTs was observed at 1641cm-1 which is attributed to C=O group [99]. In this study, The O-H (3435 cm-1) and C=O (1625cm-1) from COOH indicated the successful oxidization of SWNT. The N-H bond from DOX appears at 1545cm-1 based on reference[100]. In the current research, the bands at 3448cm-1 and 1624 cm-1 are attributed to O-H and N-H group on DOX respectively. The bands at 2896cm-1 and 1109 cm-1 are attributed to C-H and C-O-C group on PEG-CO-NHS respectively. In the IR spectrum of PEG-DOX, the C=O bonds disappeared and C=N bonds showed up at 1650 cm-1, the peak shows at 3450cm-1 is attributed to OH and N-H group. The bonds at 1639 cm-1 and 3454 cm-1 are attributed to C=O and OH group from COOH on oxidized SWNT, which indicates the successful coating of PEG- DOX onto oxidized SWNT.

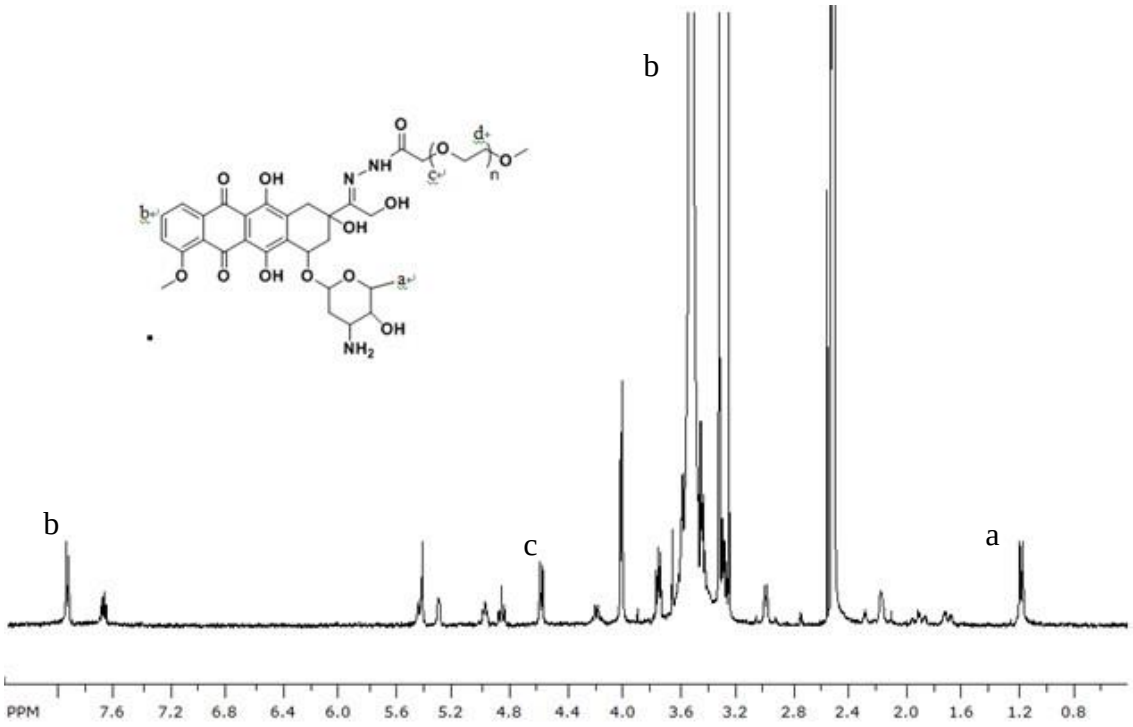


Figure 2 $^{1}$H NMR of PEG-DOX conjugate in dimethylsulfoxide-d6 (DMSO-d6)

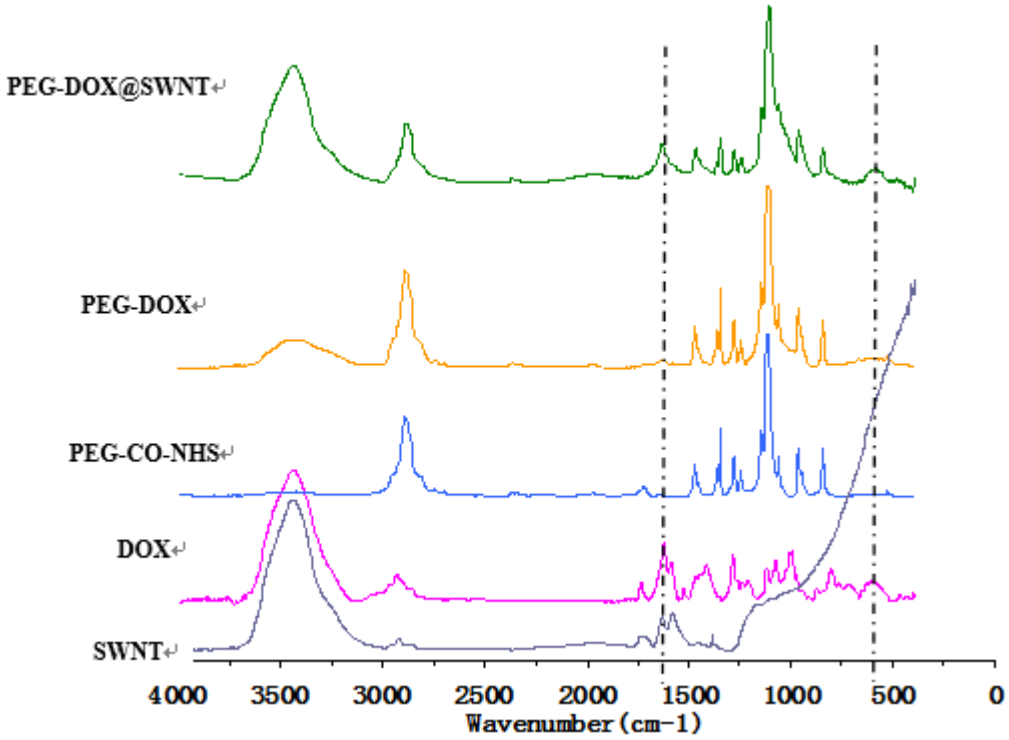


Figure 3 FT-IR comparison of doxorubicin, poly(ethylene glycol) , poly(ethylene glycol)-doxorubicin conjugates, SWNTs and PEG-DOX@SWNT hybrid micellar nanoparticle.

As shown in Figure 4, TEM image showed that the SWNTs were distinctly coated by PEG-DOX (Fig. 4 A) and in MCF-7 cell (Fig. 4 B). The size distribution and the pH-sensitive behavior of particles were investigated by dynamic light scattering (DLS). Figure 5 showed the hydrodynamic diameter of oxidized SWNTs is around 120nm. Figure 6 showed that the particle size distribution changed with the variation of pH value. At pH 7.4, the hydrodynamic diameter is around 100 nm. The hydrodynamic diameter of PEG-DOX@SWNT increased from 100 nm to 500 nm when pH changed from 7.4 to 6.0, while multiple peaks showed up at lower pH value. This can be explained by the facts that the detachment of PEG from the SWNTs resulted in the unstable dispersion of nanoparticles in aqueous solutions.

XPS was carried out in previous study, the results showed that about 4.1%-7.45% of carbon atoms are bonded with a COOH group [101-103]. In our research, XPS was conducted on oxidized SWNTs to determine content of carboxy groups on oxidized CNTs. The C 1s main peak was scanned in high resolution. In the peak fitting, the C1s core level can be broken down into four components showing at 284.6eV, 285.5eV, 286.6eV and 288.9eV. The main peak (284.6 eV) was attributed to the sp2-hybridized carbon atoms, the peak at 285.5eV was attributed to sp3-hybridized carbon atoms. The peaks at 286.6 eV and 288.9eV were assigned to –C–O and –COO− respectively. At 290.58 eV, there was the shake up characteristic typical of aromatic structures[104]. The XPS spectra are displayed in Figure 7. Table 1 showed relative percentages of the four XPS components of carbon atoms in the oxidized SWNTs. The result showed that about 6.19% of carbon atoms are bonded with a –COOH group.

The DOX loading efficiency was calculated to 31.2% in this study. The pH value and coating time may affect the drug loading efficiency. Since the π-π stacking interactions, electrostatic interaction, hydrophobic interactions, and hydrogen-bonding interaction between CNTs and DOX is stronger in pH 7.4 compare to that in acidic environment, to ensure a higher loading efficiency and remain the therapeutic characteristic of DOX at the same time, the drug loading process was conducted in the environment with neutral pH value[54]. Also, the longer loading time enable more PEG-DOX to coat onto SWNT and will result in a higher drug loading efficiency.

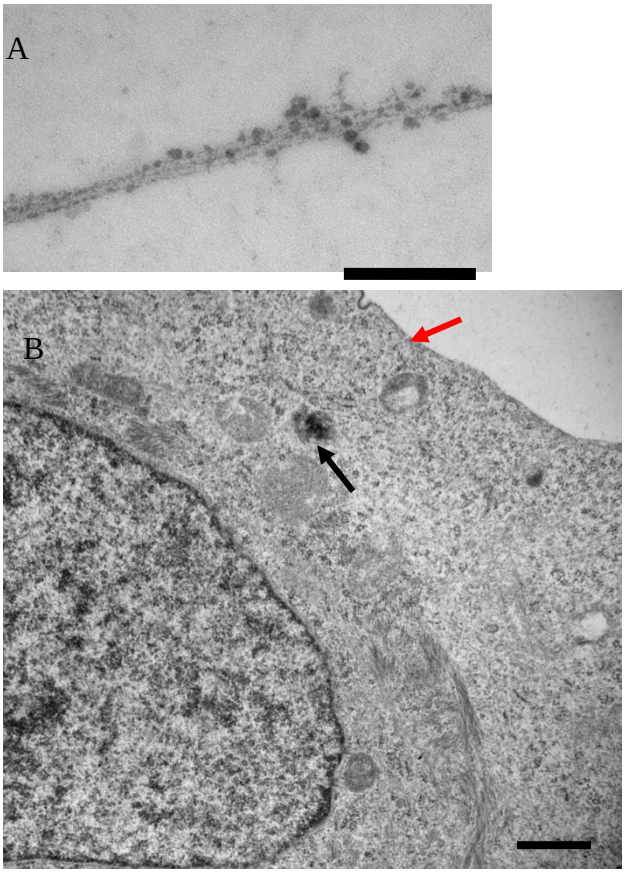


Figure 4 A. TEM image of PEG-DOX (Scale bar =20 nm). The long string like structure is SWNTs and the black dots distributed along the SWNTs are PEG-DOX. B. TEM image of MCF-7 cells incubated with PEG-DOX@SWNT. The cell membrane is showed by a red arrow, and the black area pointed by a black arrow is the PEG-DOX@SWNT. The scale bar is 500nm.

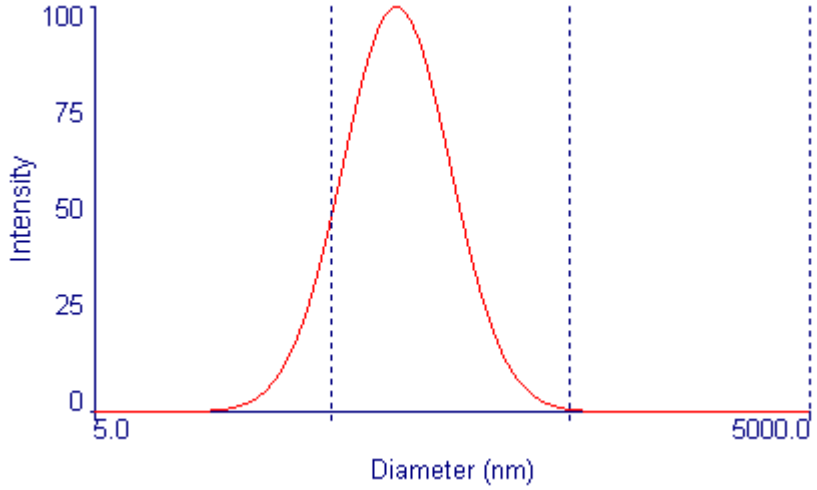


Figure 5 The dynamic light scattering (DLS) intensity distribution of oxidized SWNTs in 7.4 PBS buffer.

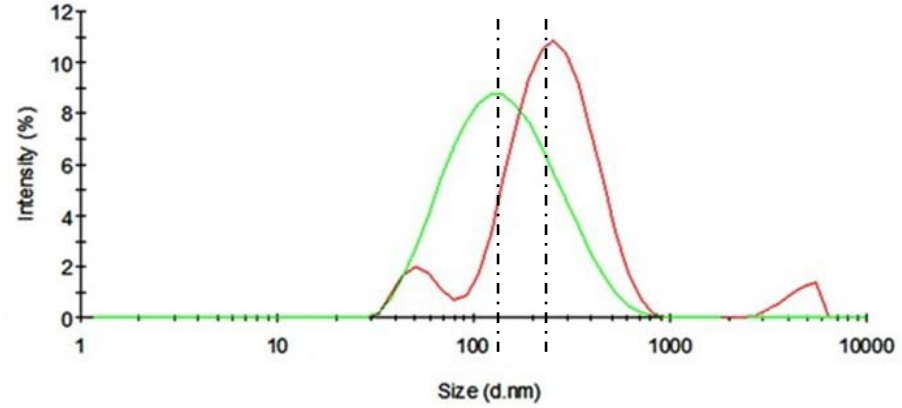


Figure 6 The dynamic light scattering (DLS) intensity distribution of PEG-DOX@SWNT in buffer with different pH. (The green line shows pH 7.4, the red line shows pH 6.0).

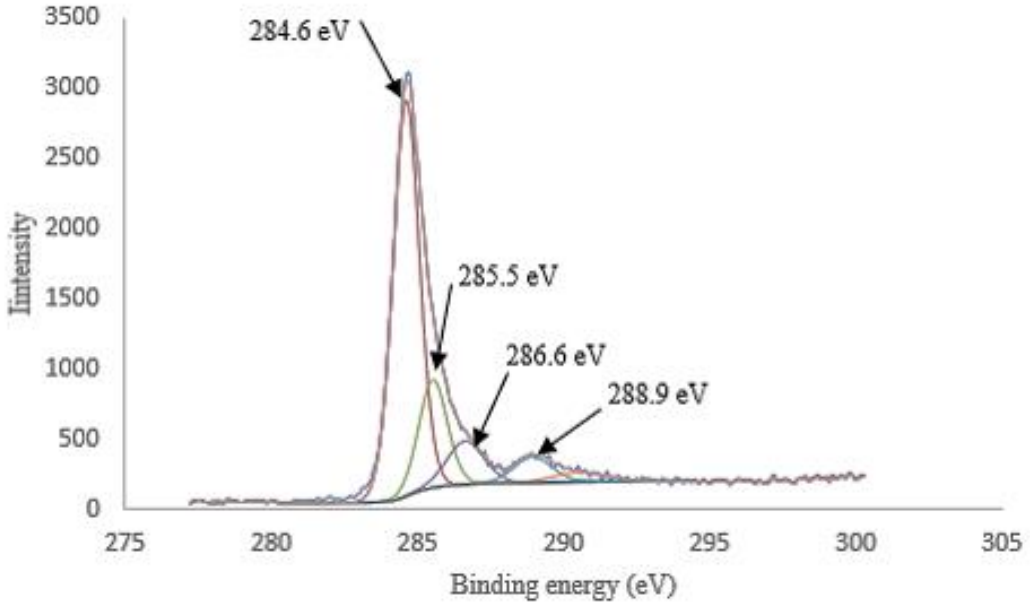


Figure 7 The XPS spectra of oxidized CNTs.

| Peak | Position(eV) | Atomic Conc. (%) |
|---|---|---|
| C 1s sp2 | 284.6 | 64.63 |
| C 1s sp3 | 285.52 | 19.05 |
| C 1s alcohol | 286.63 | 10.13 |
| C 1s acid | 288.94 | 6.19 |

Table 1 Relative percentages of the four XPS components of carbon atoms in the oxidized SWNTs.

## 4.2.2 Drug release profile

The cytosol of healthy tissues and blood has the pH value of about 7.4, and in the tumor tissues, the value ranges from 6.5 to 7.2 [105, 106]. Hence, lots of pH responsive polymeric micelles have been exploited to treat tumor tissue. The formation of hydrazone bonds is one of the general designs. Hydrazone bonds are acid-labile and through managing the length of the conjugation bonds in the

hydrazone bonds, the cleavage pH value could be easily adjusted [107-109]. In this research, the pH-dependent characteristic of hydrazone conjugation was employed for designing of a pH sensitive PEG-DOX. In addition to pH-sensitivity, it was also reported that the NIR light irradiation accelerates the release of the DOX from SWNTs [110]. In the current research, NIR light irradiation will be used as an initiator to trigger the DOX-PEG release from the PEG-DOX@SWNT hybrid micelles.

As shown in Figure 8, without NIR irradiation, DOX release was slow. About 10 % of the incorporated PEG-DOX released within 48 hours in PBS at pH 7.4. However, the DOX release from pH sensitive nanoparticles at pH 5.0 was faster, with a 7 % release in the first 6 hours and up to 17 % in 48 hours. After NIR irradiation, the rate of DOX release at pH 5.0 increased to 30% in 48 hours. Meanwhile, there was 27.7% of DOX released from NIR-pH dual sensitive nanoparticles within 48 hours in PBS at pH 7.4.

The pH sensitive and NIR sensitive release mechanism are explained as following: When the pH decrease, the protonation of –NH2 groups on DOX will be increased , which will lead the increase of hydrophilicity and the solubility of DOX, the π-π interactions is then be destroyed and DOX will be released. Which is in accordance to the previous studies conducted on pH-sensitive DOX release[54]. In addition, the pH sensitive hydrazone bonds on PEG chains will be broken and the DOX will be released. Also, when pH decrease, the acid salt from oxidized CNT will transfer to acid and the hydrogen-bonding interaction between carboxy groups and hydroxyl amino groups is weaker which will lead the release of DOX.

After irradiated by NIR, the heat transferred by CNTs from the absorbed laser energy could weaken the interaction between DOX and CNTs and render a greater amount of DOX released from the PEG-DOX@SWNTs and transfer that into heat effectively, which could trigger the release of DOX. And these results were in accordance to the previous studies on the carbon nanometerials done by other groups [111, 112]

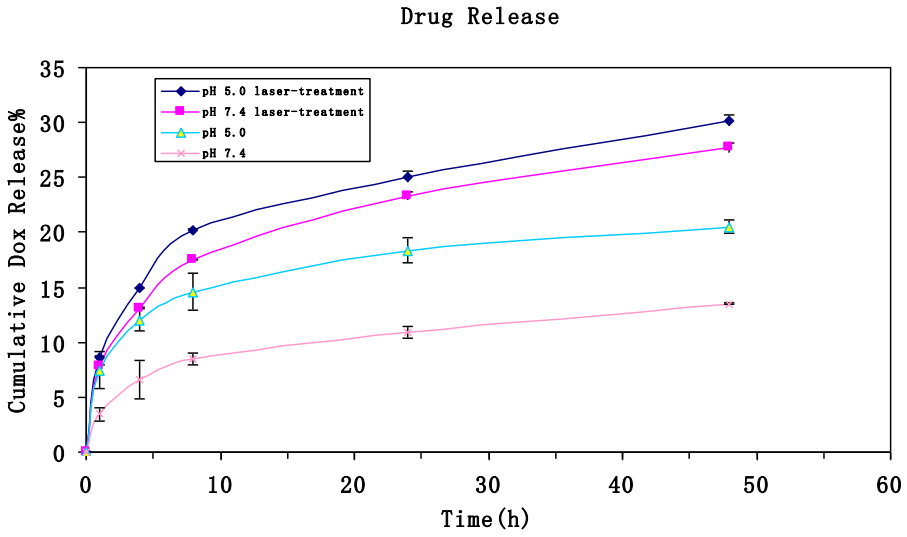


Figure 8 The cumulative drug release from NIR-pH dual sensitive nanoparticles upon NIR irradiation and pH change. Drug release increased when pH changed from 7.4 to 5.0, and after NIR irradiation the amount of DOX released highly increased in PBS at pH 7.4 and in acetate buffer at pH 5.0. (n=3)

## 4.2.3 The Multi-photon images of PEG-DOX@SWNT in MCF-7 cells

Multimodal nonlinear optical imaging microscopy (NLOM) was utilized to obtain in vitro coherent anti-Stokes Raman (CARS) and two-photon excited fluorescence (TPEF) images of MCF-7 cells with nanoparticles. The intracellular localization of the nanoparticles in live cells, and the response

of the hybrid nanoparticles toward NIR irradiation were investigated. In order to avoid the cellular damage by NIR, we used 1 mW/cm$^2$ on cells.

As shown in Figure 9, after incubation with PEG-DOX@SWNT nanoparticles for 2 hours, the DOX fluorescence in both pH 6.0 and pH 7.4 environments was found much higher than those samples incubated with only SWNTs for 2 hours. The SWNTs could absorb infrared light, which might boost the release of PEG-DOX from PEG-DOX@SWNT nanoparticles. After 24 hours of incubation, nucleuses become swollen and cytoplasm shrunk compared with those cells incubated with nanoparticles for only 2 hours (Figure 9). DOX fluorescence at pH 6.0 was significantly higher than at pH 7.4.

In order to further study after NIR on SWNTs, SWNTs without drugs were scanned by NIR laser (1 mW/cm2) for different time (0s, 20s, and 120s). It can be observed (Fig.10) that as radiation time increased, the florescence level didn't necessary increases from 20s to two minutes.

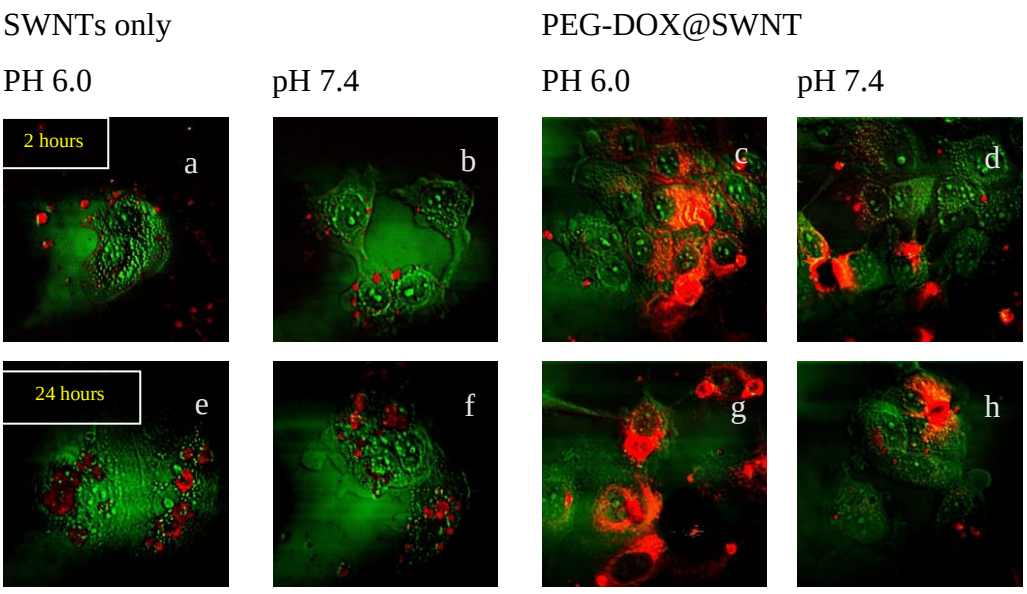

Figure 9 NLOM images of live MCF-7 incubated with SWNTs and PEG-DOX@SWNT in pH 6.0 and pH 7.4 for 1 hour (a, b, c, d) and 24 hours (e, f, g, h). The red areas in the column "PEG-DOX@SWNT" represent the two-photon excited fluorescence (TPEF) of DOX. The red areas in the column "SWNTs without DOX" represent the two-photon excited fluorescence (TPEF) of SWNTS. The green channel is Coherent anti-Stokes Raman (CARS) images, showing MCF-7 cells structures. Each image has a depth of view around 2 μm.

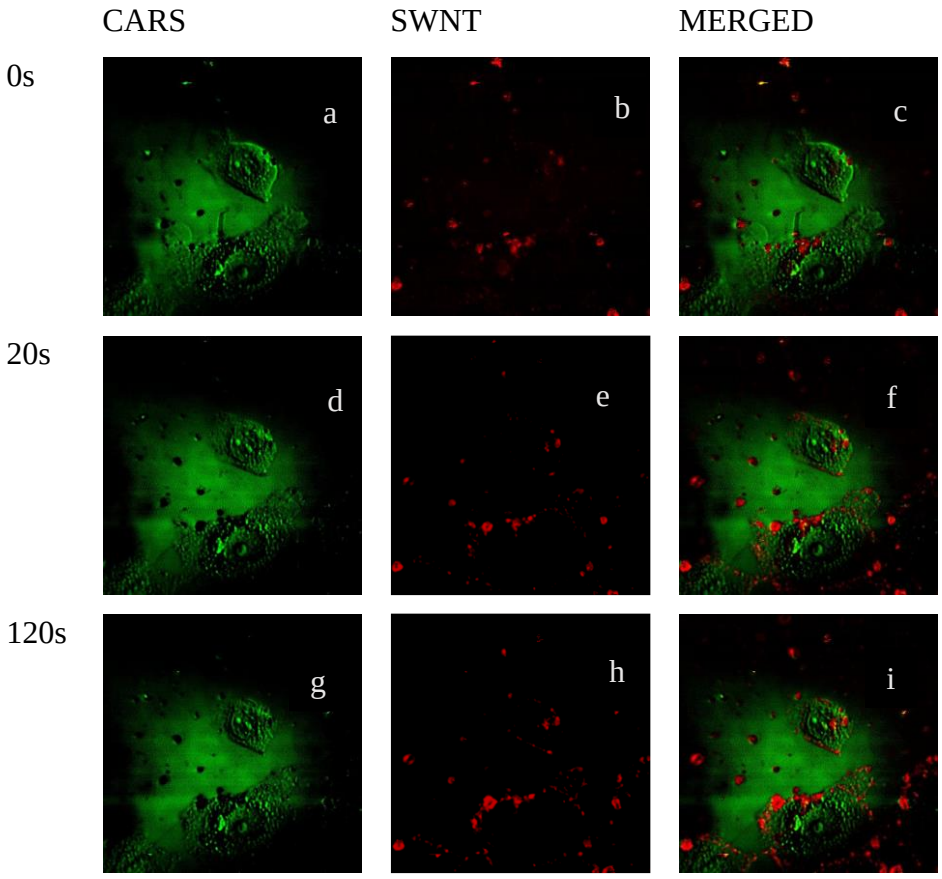


Figure 10 NLOM images of live MCF-7 after 2 hours incubation with SWNTs. Images were recorded after exposure to NIR for 0s(a-c), 20s(d-f), and 120s(g-i), the images in the middle are the two-photon excited fluorescence (TPEF) of SWNTS. The images at left are the images of Coherent anti-Stokes Raman (CARS). Each image has a depth of view around 2 μm.

In order to test the effect of NIR laser treatment (1 $mW/cm^2$) on the drug release from PEG-DOX@SWNT, the samples incubated with PEG-DOX@SWNT were treated using NIR for different time 0s, 20s, and 120s. It can be observed that the florescence intensity also increases with treating time (Fig. 11).

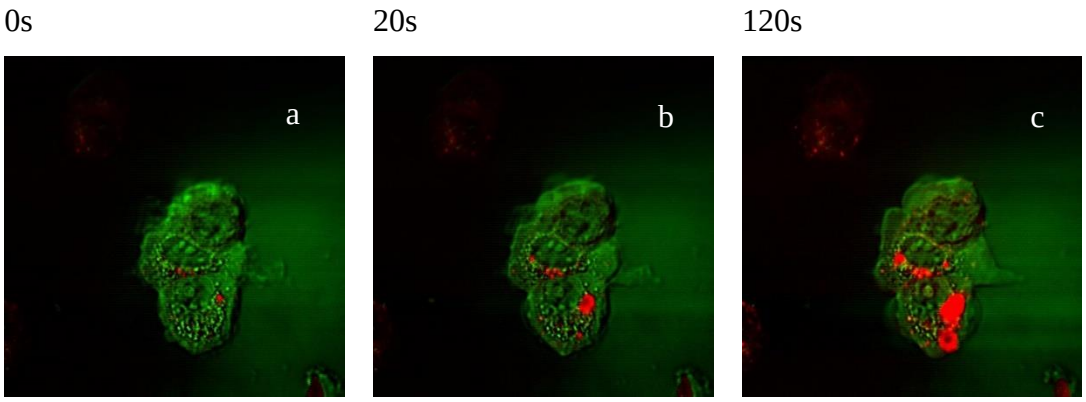


Figure 11 NLOM images of live MCF-7 after 2 hours of incubation with PEG-DOX@SWNT. Images were recorded after exposure to NIR laser for certain time: 0s(a), 20s(b), and 120s(c). The red represents the two-photon excited fluorescence (TPEF) of DOX. The green channel is Coherent anti-Stokes Raman (CARS) images, showing MCF-7 cells structures.

## 4.2.4 The confocal and TEM images of PEG-DOX@SWNT in MCF-7

The concentration of PEG-DOX@SWNT is ~1 .33mg/ml (the test concentration of DOX is ~ 5 ug/ml: Adding 100ul of solution into 1.8ml medium). As shown in Figure 12, DOX fluorescence was partially observed in and around the nuclei of the MCF-7 breast cancer cells at pH 6.0 after 15 minutes of PEG-DOX@SWNT added. After 2 hours of treatment of PEG-DOX@SWNTs, the intensity of DOX fluorescence was increased and the DOX fluorescence was found considerably

higher in the nucleus of the MCF-7 breast cancer cells. Some SWNTs were observed in cytoplasm and also outside of cytoplasm. After 24 hours of exposure with released drugs, most SWNTs were accumulated in cytoplasm. Compared with the morphologies of cells after 3 hours of incubation, the nucleuses of the cells are swollen and cytoplasm shrank. On the other hand, the cells treated with PEG-DOX@SWNT nanoparticles at pH 7.4 hardly showed the DOX fluorescence even after 24 hours incubation. But the PEG-DOX@SWNT nanoparticles were found located in the cytoplasm after 2 hours of treatment and aggregated after 24 hours. The CLSM images suggested that the doxorubicin could be efficiently released from PEG-DOX@SWNT nanoparticles in pH 6.0 environment, but not in pH 7.4 environment. Figure 13 exhibits that there is no significant difference in DOX distribution between the pH 6.0 and the pH 7.4 groups. We are following the previous studies have conducted on CNT based nanoparticles for biomedical application with respect to cell morphology test[44, 61, 63]. They mainly focused on the exploring of fluorescence images and confocal images of cell incubated with CNT based nanoparticles. We do understand the significant role flow cytometry analysis is playing and we want to conduct this experiment. Unfortunately, we are not able to do the flow cytometry analysis in our current situation but we will definitely add this analysis in our following studies for this research in the future.

PEG-DOX@SWNT

pH 6.0 pH 7.4

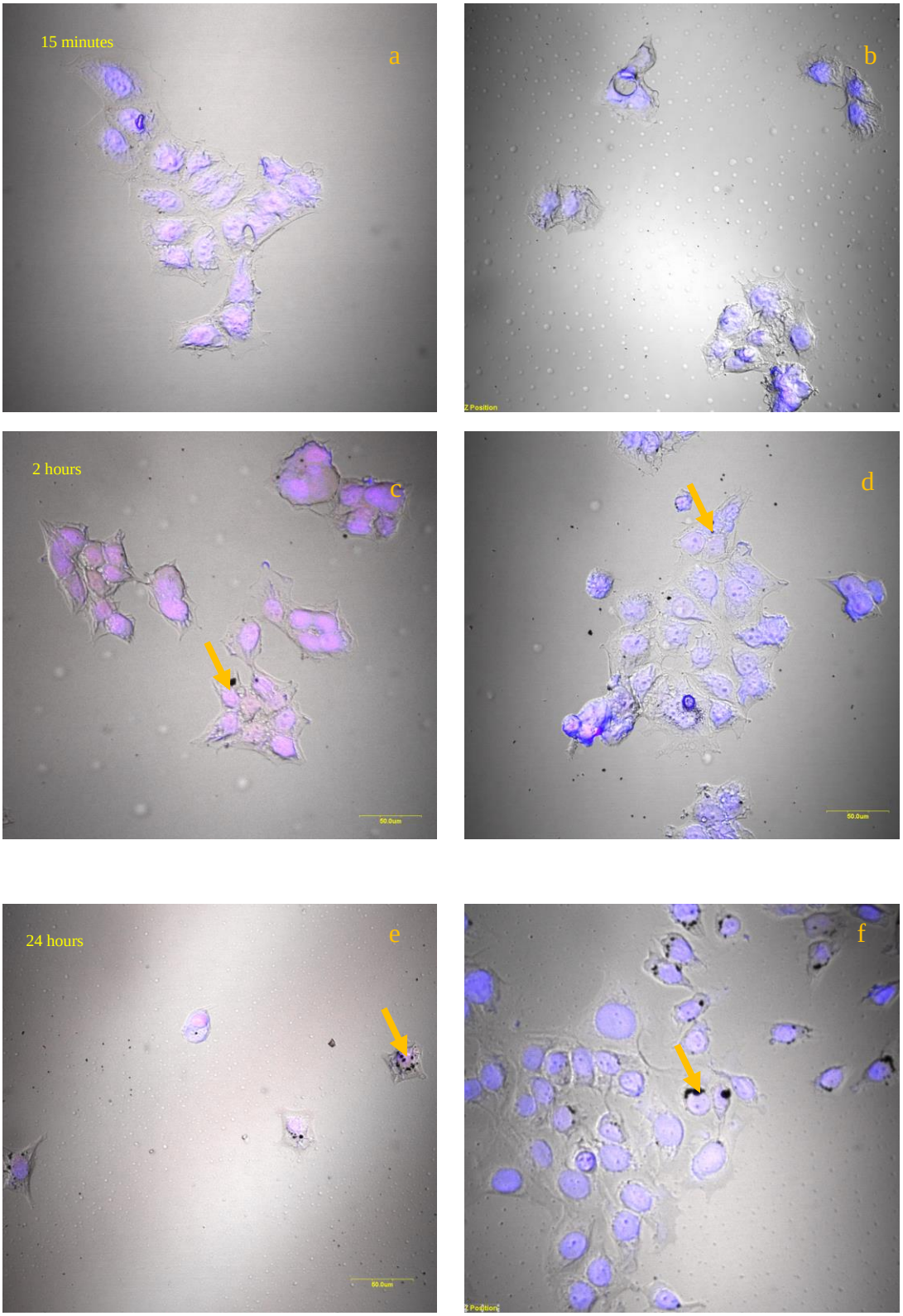


Figure 12 The bright field and confocal images of PEG-DOX@SWNT in MCF-7 cells. The MCF-7 cells were incubated with PEG-DOX@SWNT for different time: 15 minutes (a, b), 2 hours

(c, d) and 24 hours (e, f).The releasing of DOX in pH 6.0 (a, c, e) was much more efficient than that in pH 7.4(b, d ,f). Most DOX are located in the nucleus of MCE-7 cells whereas most SWNTs are located in the cytoplasm of MCE-7 cells (as showed by yellow arrow).

DOXORUBICIN

pH 6.0 pH 7.4

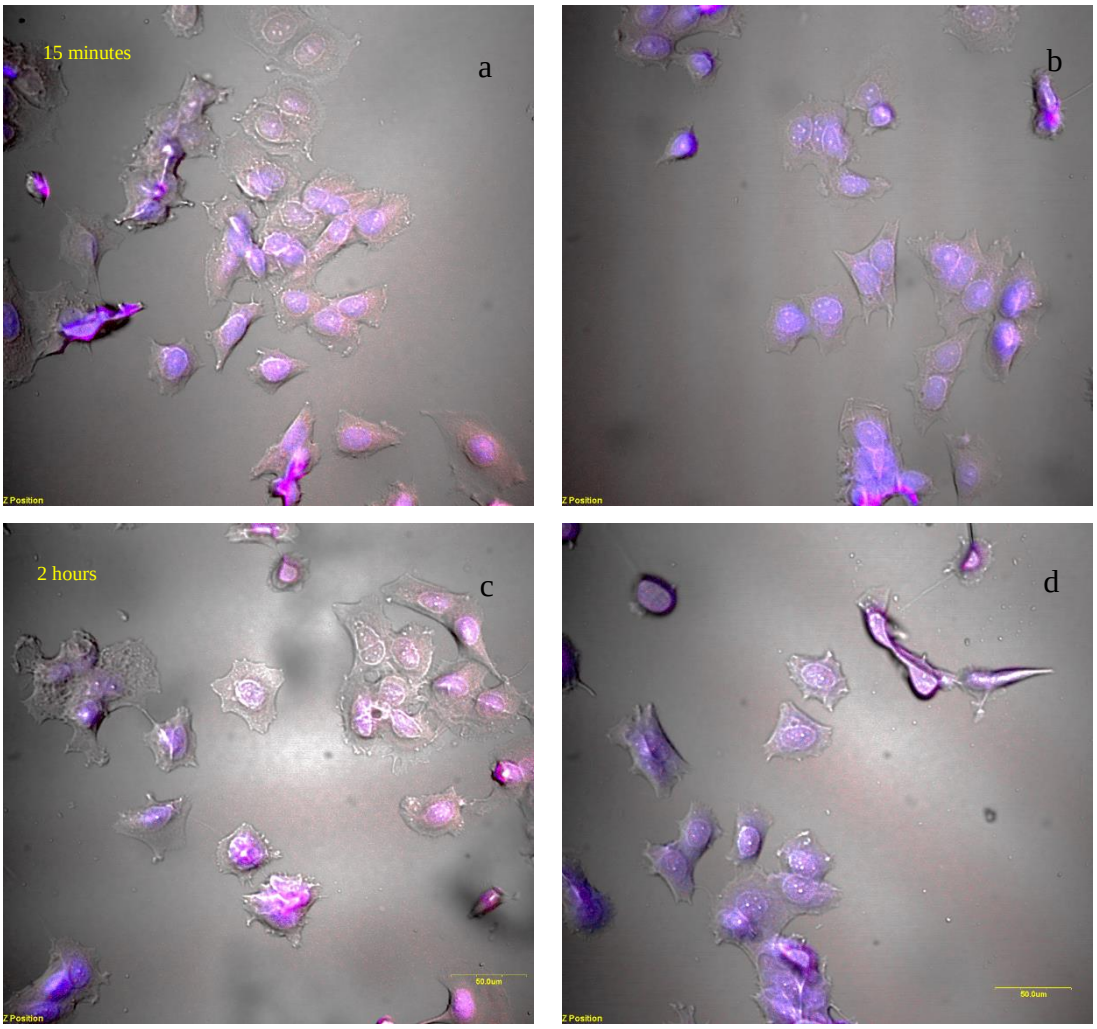

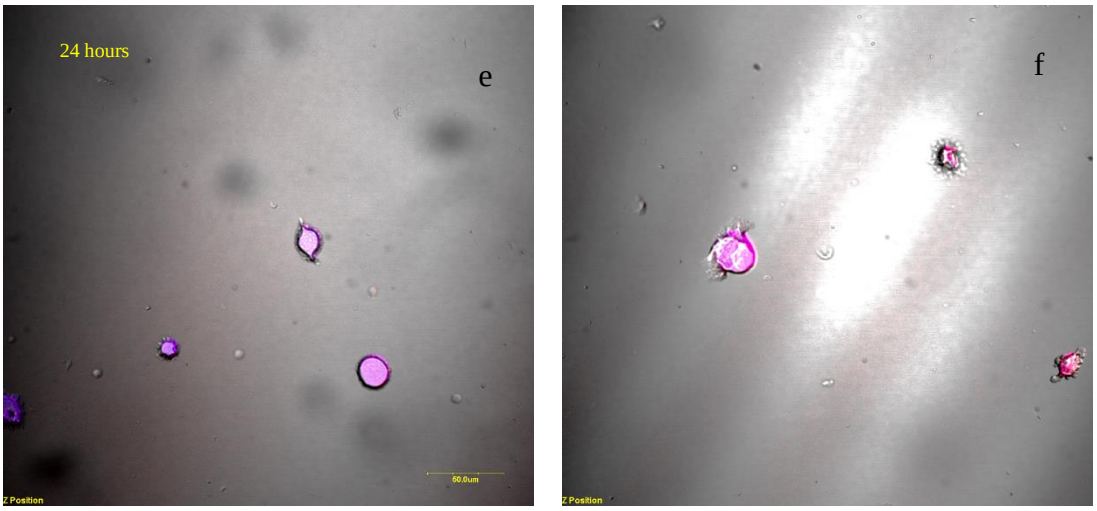


Figure 13 The bright field and confocal images of doxorubicin in MCF-7 cells. The MCF-7 cells were incubated with doxorubicin for different time: 15 minutes (a, b), 2 hours (c, d) and 24 hours (e, f). There is no significant difference in DOX distribution between the pH 6.0 and the pH 7.4 groups.

## 4.2.5 Cell viability

The cell viability was evaluated by MTT assay. Figure 14 showed in vitro cytotoxicity of PEG-DOX@SWNT on MCF-7 cells with or without NIR laser exposure. The cell viability is reduced with the treatment of laser. For cell samples with concentration of DOX at 10 ug/ml or below the viability of cells in laser treated group was almost 20 % lower than the untreated group. Such difference in cell viability was less pronounced when DOX concentration was higher than 10 ug/ml.

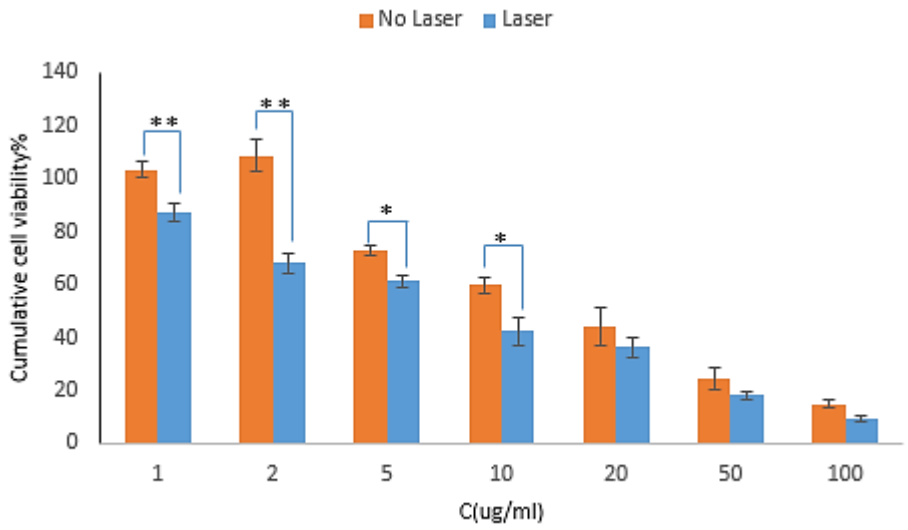


Figure 14 in vitro cytotoxicity of PEG-DOX@SWNT nanoparticles with or without laser treatment on MCF-7 cells. The results are presented as mean values of three replications and standard deviation (n=3). (“* “means $p<0.05$, “**” means $p<0.005$)

## 4.3 Summery

In this work, a pH sensitive PEG-DOX prodrug was synthesized on single wall carbon nanotubes to form the NIR-pH dual sensitive drug release system. The in vitro release of DOX from the DOX-loaded carbon nanotubes was evaluated upon laser treatment and changing pH. Multimodal nonlinear optical imaging microscopy and confocal microscopy images verified the efficacy of our anticancer drug delivery system.

# Chapter 5 Temperature sensitive single wall carbon nanotube hydrogel

## 5.1 Materials and Methods

### 5.1.1 Materials

All chemicals were purchased from Aldrich Chemical Co. (St. Louis, MO, US) and used without further purification unless otherwise mentioned. Ethyl (dimethylaminopropyl) carbodiimide (EDC) and N-Hydroxysuccinimide (NHS) were purchased from JenKem Technology USA Inc. (Allen, TX, US). Dialysis membrane (cut-off=7 kDa MWCO). N-isopropylacrylamide (NIPAM), Cysteamino hydrochloride, 3-Aminopropyl-trimethoxysilan, Ammonium persulfate(APTS), N,N,N',N'-tetramethylethylenediamine(TMED), and gelatine were purchased from ACROS (New Jersey,USA). MCF-7 cells were gifted from Dr. A Raouf (Manitoba Cancer Care).SWNT were purchased from US Research nanomaterials.

### 5.1.2 Preparation of Oxidized SWNTs

The oxidized SWNTs were prepared based on a previous research [19]. Basically, the solution contained 98 % H2SO4 and 65 % HNO3 with volume ratio of 3 to 1 was first prepared. 50 mg of

SWNTs was then added into the solution, the mixture was then sonicated for 24 hours at 0 °C. Ultrapure water (18.2 MΩ) was then utilized to rinse the oxidized SWNTS for five times. The mixture was next centrifuged with the speed of 13000rpm for 3 times with each time for 10min. The oxidized SWNTs were collected from deposit and the black powder was gained by lyophilization.

### 5.1.3 Preparation of SWNT-APTS composite

100mg of SWNTs were added into the solution of 10g 3-Aminopropyl-trimethoxysilan, 100ml ethanol (95%) and 1ml acetic acid (99.7%). Then the mixture was ultrasonic for 10mins following by 30mins centrifuge. The centrifuge was repeated for 3 times with the speed of 10000rpm, each round was last 10mins and the composite was rinsed with DD water for three times. The black powder of SWNT-APTS collected from deposit was obtained by lyophilisation. The preparation of SWNT-APTS was verified by FTIR test. Fourier transform infrared spectroscopy (FTIR) test was adopted applying an IR Spectrophotometer (Bruker IFS 66v/s, German) within limits between 4000–400 cm−1.

### 5.1.4 Preparation of Gelatin/SWNT-APTS composite

1g gelatin was dissolved in 100ml Trifluoroethanol (TFE) for 24hrs. 60mg black powder of SWNT-APTS was then added to the 100ml gelatin solution (1%) followed by 30mins ultrasonic. The solution was stirred for 24hs, and was subsequently centrifuged for 1 h. The centrifuge was repeated for 3 times at the speed of 12000rpm, with each round lasting for 20mins. After that, the composite was washed by DD water for three times, and the deposit was collected.

Gelatin/SWNT-APTS was collected after dried in high vacuum for 24 h. The preparation of Gelatin/SWNT-APTS was verified by FTIR test.

### 5.1.5 Synthesis of pNIPAM-$NH_2$ composite

The mixture of 550mg NIPAM, 25mg Cysteamine, 100ul APS and 6ml Milli-Q water was heated to 70°C for 3h in nitrogen. The solution was then dialyzed against Milli-Q water for 2 days. The PNIPAM-NH2 polymer was collected through lyophilisation. The synthesis of PNIPAM-NH2 polymer was verified by FTIR test.

### 5.1.6 Preparation of Gelatin/SWNT-APTS-$NH_2$ nanoparticles

10mg Gelatin/SWNT-APTS composite was dispersed in the solution consisted of 10ml 7.4 PBS buffer (0.1M), 120mg EDC and 70mg NHS to cross link gelatin onto SWNT. The mixture of 154mg PNIPAM-NH2 and cross-linked Gelatin/SWNT-APTS were then centrifuged in 40°C. The final product was obtained by lyophilisation. The preparation of Gelatin/SWNT-APTS-NH2 was verified by FTIR.

### 5.1.7 Rheological experiment of Gelatin/SWNT-APTS-$NH_2$

Rheological test of Gelatin/SWNT-APTS-NH2 were carried out with an AR 2000 advanced rheometer (TA Instruments). The viscoelastic properties of SWNT-based thermo-sensitive hydrogel were tested through their rheological properties during its formation. In the oscillation procedure, gap was 52.00 micro meters and 20mm 1° steel cone was applied. Compression distance, compression velocity and shear rate factor of rheological experiment was set to be 119.0 micro

meters, 3000.0 micrometers and 57.29 respectively. Sample volume was approximately 40ul. The temperature was increase from 27°C to 45°C with a rate of 3.00°C/min and the frequency was 1 Hz. The storage modulus (G') and the loss modulus (G") were obtained.

### 5.1.8 Cell viability assay of cells incubated with thermo-sensitive gel

The cytotoxicity of the thermo-sensitive gel with or without laser treatment was investigated by a methylthiazoltetrazolium bromide (MTT) assay. MCF-7 breast cancer cells were cultured with DMEM (containing 10% FBS), $1.0\times10^5$ U/l penicillin and 100 mg/l streptomycin at 37 °C in 5 % CO2. MCF-7 breast cancer cells were seeded in a 96-well tissue culture plate with culture density of 8,000 cells per well. After 24hs, the growth medium was removed and fresh DMEM was added. Then the gel precursor with or without laser treatment were added into the wells. 10 μL MTT solutions were added after 24 h incubation, and the cells were incubated for 4hs. 200ul DMSO was next added into wells to dissolve formazan. ELISA plate reader was then applied to examine the absorbance of wells at wavelength of 570 nm and 630 nm. The cell viability was then calculated.

## 5.2 Results and discussion

### 5.2.1 The gel formation of NIPAM-$NH_2$ and Gelatin/SWNT-APTS-$NH_2$

pNIPAM is known as a thermo sensitive polymer. When the temperature is lower than its lower critical solution temperature( 33℃), the H-bond between N, O atoms from amid bonds and water molecules will be formed, when the temperature is higher than lower critical solution temperature,

the H-bond will be damaged, thus the polymer chain will transform to a coiled structure. The SWNT can disperse in the solution of pNIPAM in low temperature because the amphiphilic polymer chain of pNIPAM can adhere onto the surface of SWNT. When the temperature is higher than 33°, the SWNT will aggregate into little trusses due to the contraction of pNIPAM polymer's chain conformation and the hydrophobic SWNT surface will be revealed to water. Figure 14a shows the NIPAM-$NH_2$ solution in room temperature, when temperature is higher than lower critical solution temperature of NIPAM(33℃), the NIPAM-$NH_2$ hydrogel is formed (b), and after the temperature is decreased the hydrogel will turn to solution again. The gel formation test was employed on Gelatin/SWNT-APTS-$NH_2$ nanoparticle as well and it turned out that the Gelatin/SWNT-APTS-$NH_2$ hydrogel was formed when temperature was higher than 33℃(Figure 15). This gel formation behavior is also reversible.

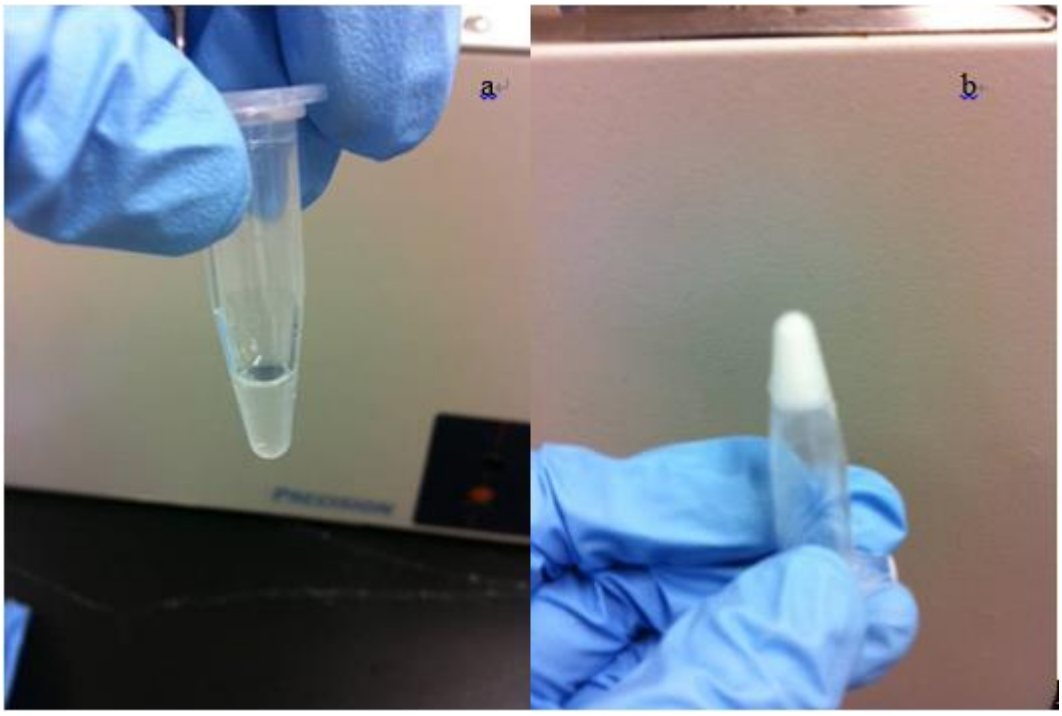


Figure 15 The gel formation image for NIPAM-$NH_2$. Image a was taken in room temperature. Image b was taken after 1min heat in 37℃ water bath.


Figure 16 the gel formation image for Gelatin/SWNT-APTS-$NH_2$. Image a was taken in room temperature. Image b was taken after 1min heat in 37 ℃ water bath.

## 5.2.2 The characterization of Gelatin/SWNT-APTS-$NH_2$

Fourier transform infrared spectroscopy (FTIR) was employed for the characterization of Gelatin, SWNT-APTS, Gelatin/SWNT-APTS, NIPAM, pNIPAM-$NH_2$ and Gelatin/SWNT-APTS-$NH_2$. As shown in Figure 16, the band at 1104 $cm^{-1}$ displayed in the spectrum of Gelatin/SWNT-APTS are attributed to Si-O-Si resulted from SWNT-APTS. The band at 1103 $cm^{-1}$ shown in the spectrum of Gelatin/SWNT-APTS-$NH_2$ was attributed to Si-O-Si from Gelatin/SWNT-APTS. As exhibited in Figure 16, we concluded that Gelatin/SWNT-APTS-$NH_2$ was successfully prepared from Gelatin/SWNT-APTS and pNIPAM-$NH_2$.

.

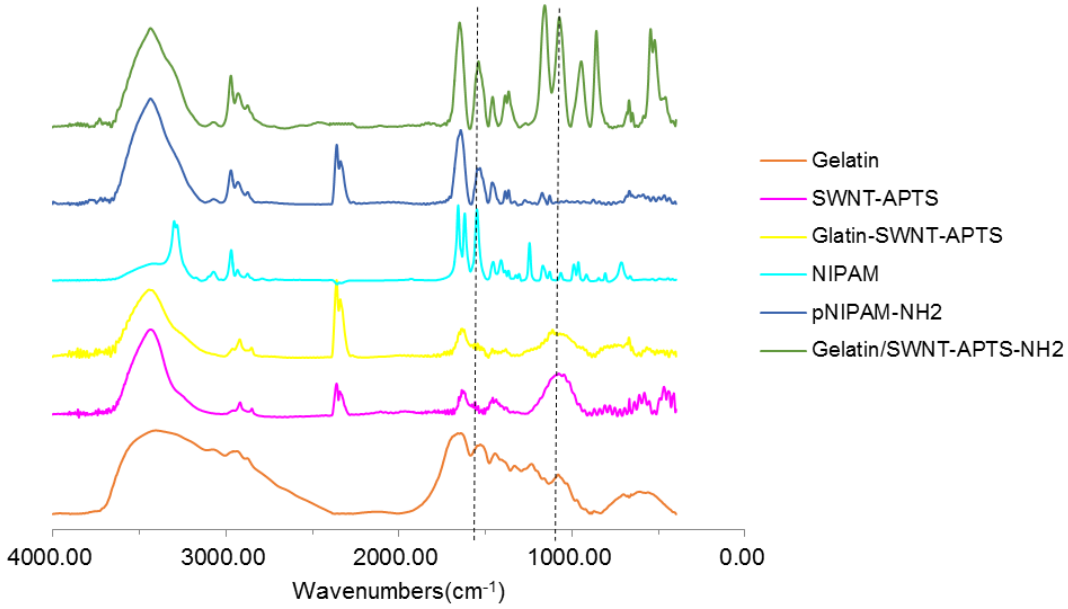


Figure 17 FT-IR comparison of Gelatin, SWNT-APTS, Gelatin/SWNT-APTS, NIPAM, pNIPAM-$NH_2$ and Gelatin/SWNT-APTS-$NH_2$.

## 5.2.3 Cell viability

The cell viability was determined by MTT assay. Figure 17 showed the in vitro cytotoxicity of thermo-sensitive hydrogel on MCF-7 cells with or without laser scanning. The laser treatment barely has any influence on the cells from control group. After incubated with thermo-sensitive hydrogel, the cell viability reduced with the treatment of laser, when the concentration of SWNT is 10 mg/ml the viability of cells in 3mins laser treatment group was almost 50 % lower than no laser treatment group. It was also shown that there was no obvious difference in cell viability between 15s treatment

group and 3mins treatment group, therefor, there is no need to increase laser treat time from 15s to 3mins.

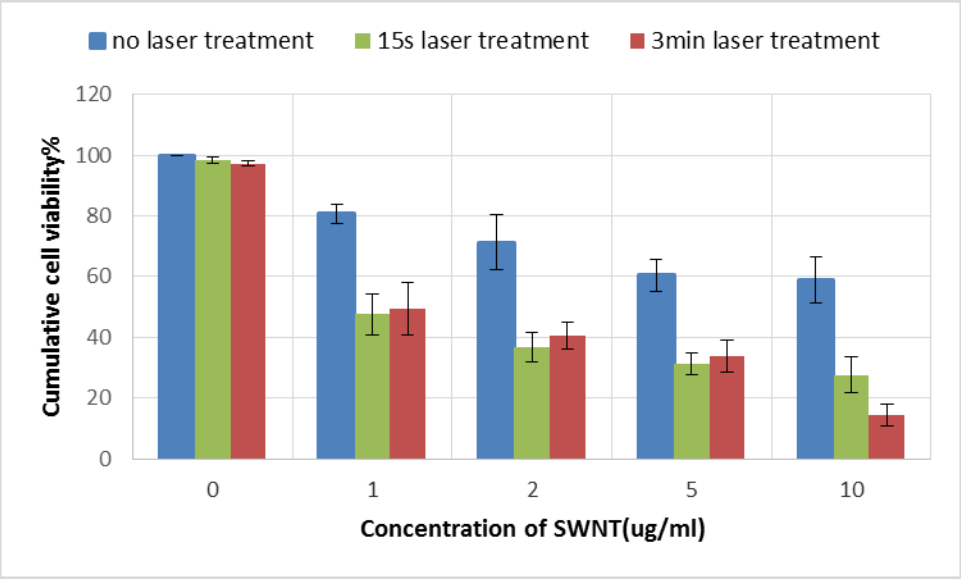


Figure 18 The in vitro cytotoxicity of Gelatin/SWNT-APTS-$NH_2$ hydrogel with or without laser treatment on MCF-7. The results are presented as mean values of three replications and standard deviation.

## 5.2.4 Rheology test

It is reported that the storage modulus (G') and loss modulus (G") are very crucial parameters of materials. If the storage modulus is lower than loss modulus, the material shows a liquid form, when the storage modulus is higher than loss modulus, the material shows a hydrogel form [113]. A rheology meter was used to test the storage modulus and loss modulus of Gelatin/ SWNT-APTS-NH2 hydrogel. As can be seen in figure 18, both the storage modulus and loss modulus increase with test temperature, when the temperature was lower than 36.5 °C, the storage modulus was lower than loss modulus which indicate that the material exhibit a liquid form; when the temperature was

higher than 36.5 °C the storage modulus was higher than loss modulus which indicate that the Gelatin/SWNT-APTS-NH2 hydrogel was formed. The modules decrease when temperature was higher than 42.5 °C which is probably due to that the hydrogel is very weak and when temperature was higher than 42.5 °C the structure of hydrogel was broken and result in the decreasing modules.

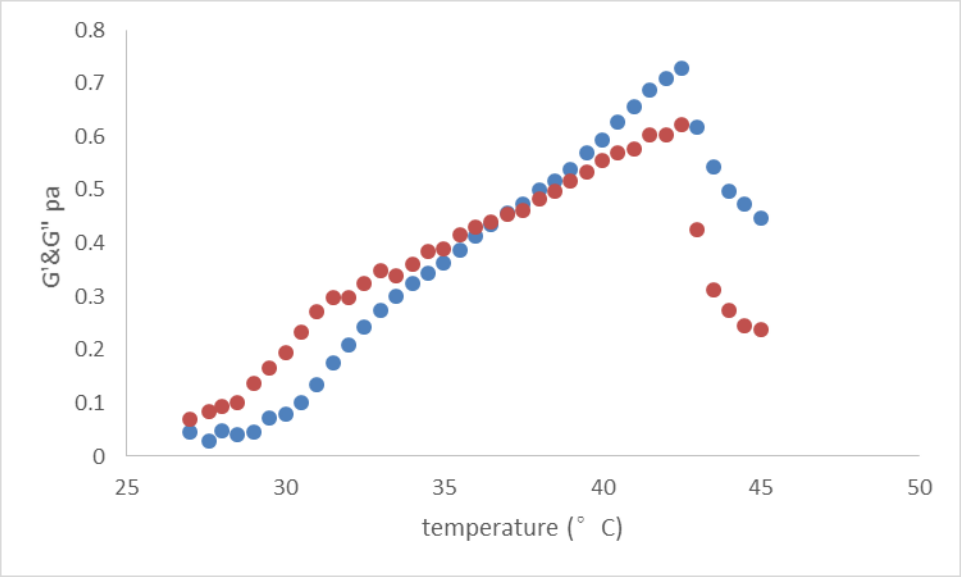


Figure 18 Rheological properties of thermosensitive Gelatin/SWNT-APTS-NH2 hydrogel, the blue dots represent storage modulus and the red dots represent loss modulus.

## 5.3 Summery

In this work, a thermo-sensitive Gelatin/SWNT-APTS-$NH_2$ hydrogel was synthesized and its effectiveness of inhibiting cancer cells through the exposure of SWNT based thermo-sensitive hydrogels to NIR was tested. When temperature was higher than 33 centigrade the hydrogel was formed, when temperature decrease to room temperature the hydrogel turned into a solution, as demonstrated by pictures captured by digital camera. The MTT assay results show that the viability of MCF-7 cancer cells was highly reduced after treated by NIR laser treatment. Thermogravimetric analysis (TGA) of SWNT, SWNT-APTS, Gelatin /SWNT-APTS, Gelatin/SWNT-APTS-$NH_2$

nanoparticles, gelatin and NIPAM were tested with 20 mg of each sample on a Setaram Setsys 16 thermal analyzer (France) in N2 from 25 to 1000 °C at a invariable heating rate of 2 °C min−1. Rheological test of Gelatin/SWNT-APTS-NH2 was carried out with an AR 2000 advanced rheometer (TA Instruments). The viscoelastic properties of SWNT based thermo-sensitive hydrogel were tested through determining their rheological properties applying hydrogel at a constant concentration of 2% w/v.

# Chapter 6 Silica coated magnetic nanoparticles for cancer treatment

## 6.1 Materials and Methods

### 6.1.1 Materials

Iron (II) sulfate heptahydrate, Iron (III) chloride hexahydrate were purchased from Sigma-Aldrich Corporation. Dialysis membrane (cut-off=7 kDa MWCO). Pluronic F-127, gelatine and glutaraldehyde were purchased from ACROS (New Jersey,USA). SWNT purchased from US Research nanomaterials were used without further purification. Bone marrow stromal cells (BMSC) cells were purchased from ATCC.

### 6.1.2 Synthesis of magnetic nanoparticles

The $Fe_3O_4$ nanoparticle were synthesized according to reference[114]. Basically, 0.43g Iron (II) sulfate heptahydrate were dissolved in 35ml DD water. 1.98g Iron (III) chloride hexahydrate were dissolved in 4ml 1.5M HCL solution. Subsequently, 35ml $Fe(SO_4)\cdot 7H_2O$ solution, 1.7ml

$FeCL_3 \cdot 6H_2O$ solution and 3ml $NH_3H_2O$ were mixed together, following by 15mins strong stirring and serve for 24hs. Magnetic nanoparticles were obtained after washed by DD water for 3 times.

### 6.1.3 Prepare APTS-coated magnetic nanoparticles

The synthesis of APTS-coated magnetic nanoparticles followed the reference [115] with modification. Briefly, 1g APTS was mix with 10ml 95% ethanol and 100ul acetic acid (99.7%). 74mg $Fe_3O_4$ nanoparticles were then added into mixture and sonicated for 3hs following by 24hs stirring. The black powder was collected by centrifuge and then dried in high vacuum for 24 h.

### 6.1.4 Prepare APTS-$Fe_3O_4$ magnetic hydrogel

200mg SWNT were added into 20ml Pluronic F-127 solution and sonicated for 3hs until homogeneous solution was obtained. Dissolve 20g gelatin in 100ml Trifluoroethanol (TFE) for 24hs. Mix 12mg APTS-coated magnetic nanoparticles, 1ml gelatin solution and 1ml SWNT solution together, then the mixture was sonicated for 1hs. After that, 40ul glutaraldehyde was added into 300ul mixture. The SWNT /Gelatin-APTS-Fe3O4 magnetic hydrogel was obtained after 30mins. 300ul 5% NaBH3CN solution wad next used as reducing agent and be removed after 30mins. DD water was then added to wash hydrogel for three times. The final product was obtained by lyophilisation.

### 6.1.5 Determination of APTS-$Fe_3O_4$ magnetic hydrogel

Fourier transform infrared spectroscopy (FTIR) test was carried out on an IR Spectrophotometer (Bruker IFS 66v/s, German) within limits between 4000–400 cm−1. The morphology of APTS-$Fe_3O_4$ magnetic hydrogel were determined by a Joel 1010 Scanning Electron Microscope

(SEM), setting accelerating voltage at 80 KV, employing a LaB6 filament and equipped with an AMT digital camera. Micrographs were acquired at 60,000× magnification.

### 6.1.6 Hydrogel morphology test

The morphology of the hydrogel was examined by cryosection. The hydrogel was first put into 7.4 PBS buffer solution and reserve for 24hs. The hydrogel was next stained by BODIPYFL phallacidin solution for 30mins in dark, PBS was then used to wash the hydrogel for three times. Next, an O.C.T. compound was utilized to fix hydrogel in cryomold. Move O.C.T. compound to -80℃ freezer when it turns to solid form in -20℃ cryomold. Then the hydrogel was moved from cryomold to cryostat and slides were next collected.

### 6.1.7 Mechanical test of SWNT-Gelatin-F127CT hydrogel

The TA.XT2i Texture Analyzer (Texture Technologies Corp.) was utilized to determine the mechanical characteristic of SWNT/Gelatin-APTS-Fe3O4 magnetic hydrogel. Samples were prepared for the test with the following methods: three pieces of hydrogel with cylinder shape were prepared by cutting blade, the diameters of hydrogels were 12mm and the heights were 5mm. The range of mechanical test was 2.5 mm and the speed of test was 0.5mm/second. The mechanical properties of hydrogel was automatically analysed by Analyzer software. All of mechanical were conducted in room temperature.

## 6.1.8 Hydrogel for cell culture

The magnetic hydrogel used for cell test was prepared through the addition of 100ul hydrogel solution onto a piece of glass cover slip which is then covered by another glass cover slip. The cover slips were taken away after the successful gelation, then the hydrogel was immersed in 7.4 PBS buffer for 24hs. 7.4 PBS buffer was used to wash the hydrogel for three times. Next the sterilization of hydrogel was achieved through exposure to UV light in the bio-safety hood for 1h. The magnetic hydrogel was then put in culture dish. Agarose gel was first coated on culture to prevent cell attachment to the dish.

## 6.1.9 Cell morphology test

Confocal laser scanning microscopy (CLSM) was employed to examine the cell morphology of BMSC cells after incubated with SWNT/Gelatin-APTS-Fe3O4 magnetic hydrogel in PBS buffer at pH 7.4 (0.1 M) for 24 h. Firstly, the BMSC cells were seeded on the magnetic hydrogel with the cell concentration of 2 x 105 cells/dish, and the hydrogel-laden cells were cultured for 24hs. Then, cold PBS buffer was used to wash the hydrogel for three times after preconcerted incubation time. 4 % paraformaldehyde PBS solution was next utilized to make the treatment cells fixed, then the hydrogel was washed with PBS buffer for three times after 15 min incubation. The 0.1 % Triton X-100 PBS buffer was next used to perform permeabilization, then hydrogel-laden cells were incubated for 10 min following by three times wash with PBS buffer. 10 nM phallacidin/1 % (w/v) BSA solution was then utilized to dye the F-actin of the cells for 20 min to visualize the cell skeleton of BMSC cells, then hydrogel-laden cells were washed with PBS buffer for three times. The cells were then incubated in 10 nM Topro-3 for 20 min to visualize the cells nuclei was

performed and then they were rinsed with PBS buffer for three times. Finally, hydrogel-laden cells were fixed on glass slide and covered by cover slip to be observed through CLSM.

### 6.1.10 Cell viability assay of cells incubated with APTS-$Fe_3O_4$ magnetic hydrogel

The cytotoxicity of the released cells incubated with APTS-$Fe_3O_4$ magnetic hydrogel was investigated by applying a methylthiazoltetrazolium bromide (MTT) assay. Firstly, the hydrogel was prepared in 96-well tissue culture plate. BMSC cells were then cultured with DMEM(GIBCO) contained 10% FBS( GIBCO), $1.0\times10^5$ U/l penicillin (Sigma) and 100 mg/l streptomycin (Sigma) at 37 °C in 5 % $CO_2$. Then, BMSC cells were seeded on the APTS-$Fe_3O_4$ magnetic hydrogel in 96-well tissue culture plate and incubated for predetermined time with the cell concentration of 8,000 cells per well. 10 μL MTT solutions were next added to each well after 24hs and 48hs of incubation time, and cells were then incubated for 4 h. The medium was next taken out following by the addition of 200 μL DMSO. The absorbance was employed applying an ELISA plate reader at a test wavelength of 570 nm and a reference wavelength of 630 nm. The cell viability of samples was then calculated.

## 6.2 Results and discussion

### 6.2.1 The characterization of APTS coated $Fe_3O_4$ magnetic hydrogel

The infrared (FT-IR) spectroscopy was employed for the characterization of $Fe_3O_4$ magnetic nanoparticles and APTS coated nanoparticles. According to previous study, Fe-O vibration should

appears at 632cm-1 and 585 $cm^{-1}$ [116].As shown in Figure 19, the peaks at 629.9 $cm^{-1}$ and 584.5 $cm^{-1}$ were attributed to Fe-O bond. After coated with APTS, the peak appearing at 1100–900 cm−1 is assigned to Si-O bond based on one literature[116]. In the current study, the C-H vibration appeared at 2921.4 $cm^{-1}$ and 2850.7$cm^{-1}$. The band at 1003.5 $cm^{-1}$ is assigned to Si-O bond. Accordingly, in this study, APTS coated $Fe_3O_4$ magnetic nanoparticles were successfully prepared.

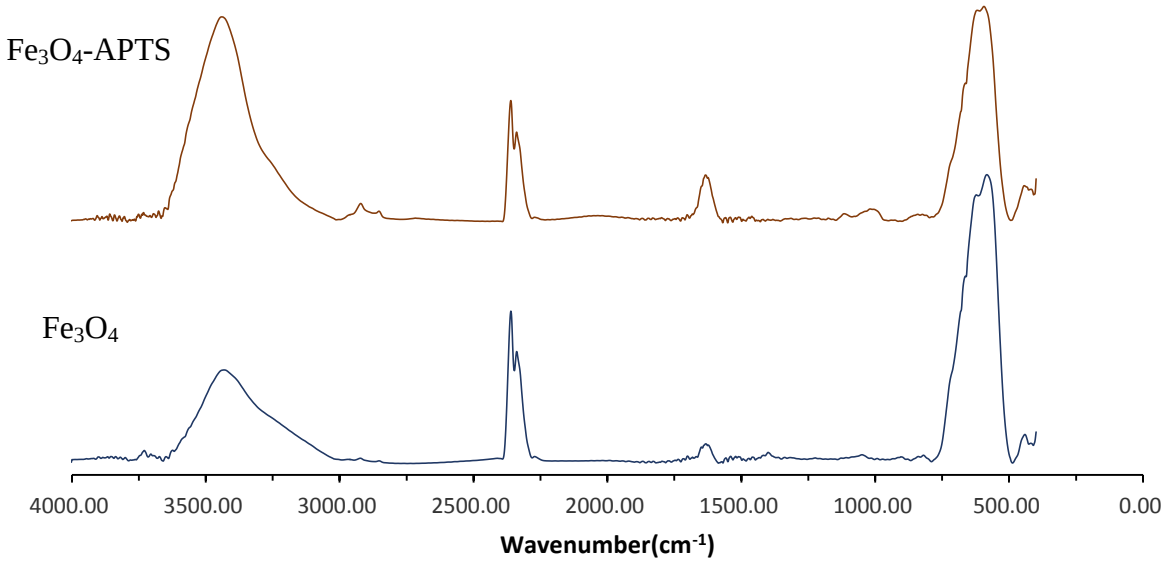


Figure 19 FT-IR comparison of blank $Fe_3O_4$ nanoparticles and the APTS-coated $Fe_3O_4$ nanoparticles.

As shown in Figure 20 and Figure 21, SEM picture shown the porous cross-section of APTS-$Fe_3O_4$ nanoparticles hydrogel. The freeze-dried APTS-$Fe_3O_4$ nanoparticles hydrogel exhibit a structure with pores. It can be revealed that the pores of hydrogel are regularly distributed in hydrogel.

As can be seen in Figure 22, the cryosection image of APTS coated magnetic nanoparticles was shown clearly. The pores of magnetic gel were evenly distributed in the hydrogel. After being immersed in PBS for 24h. The pore size of hydrogel seen from the image varied between 20um~50um.

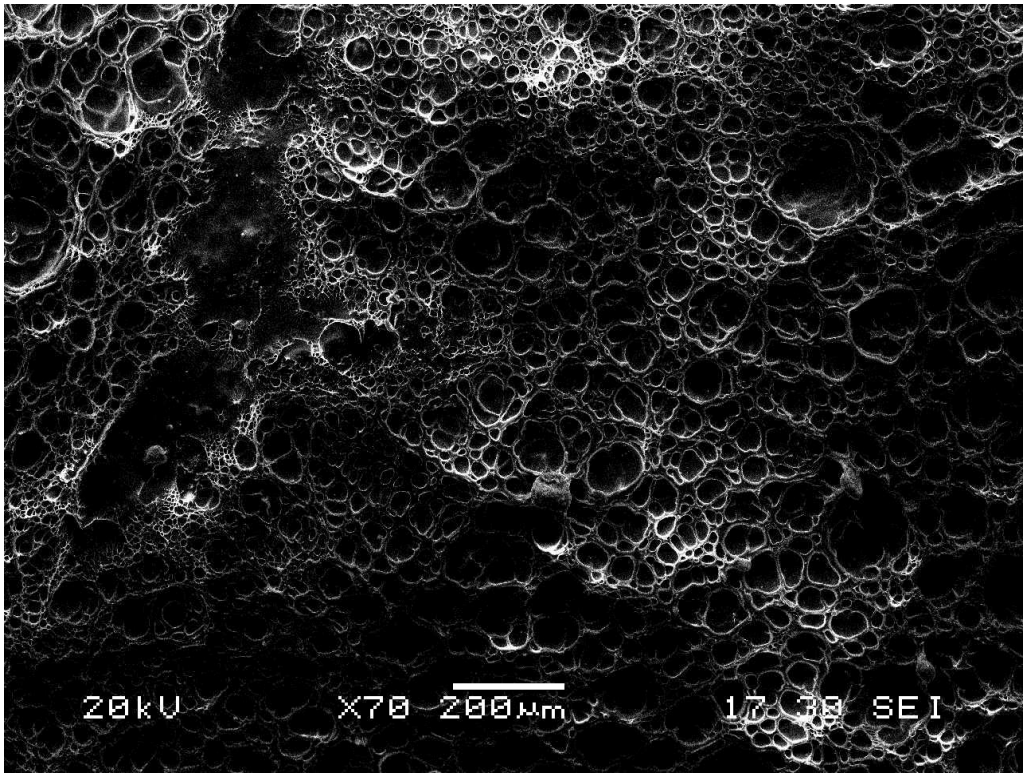


Figure 20 The SEM image APTS coated magnetic nanoparticles (Scale bar =200 um).

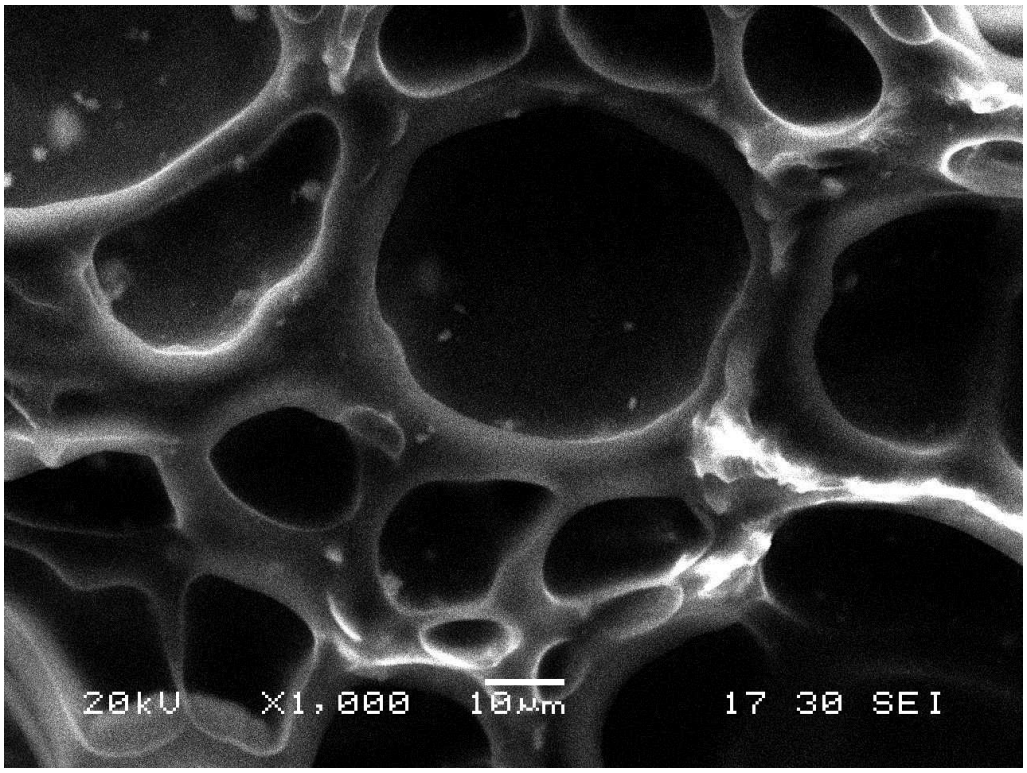


Figure 21 The large magnification SEM image APTS coated magnetic nanoparticles (Scale bar =10 um).

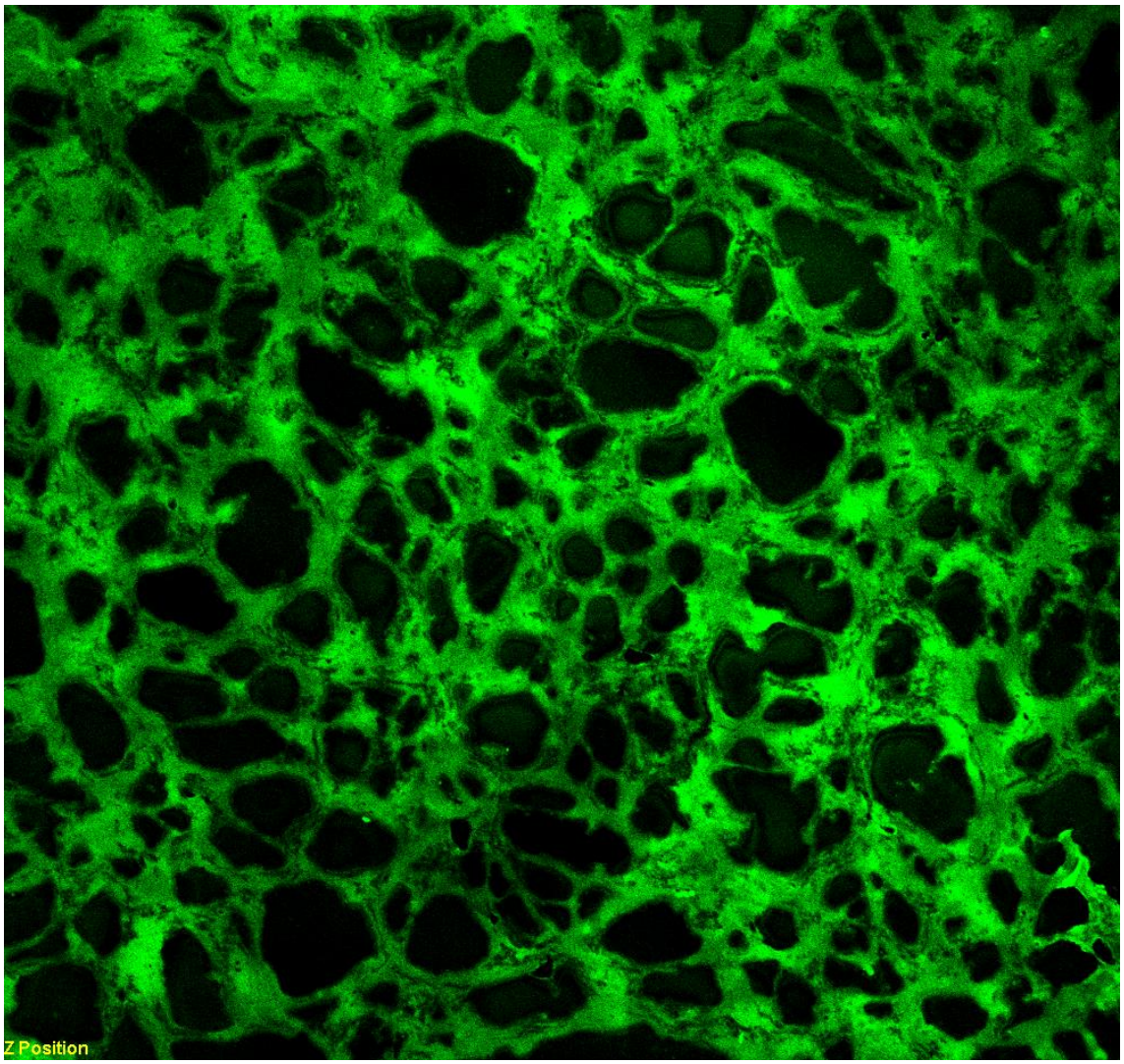


Figure 22 Cryosection images of APTS-$Fe_3O_4$ nanoparticles hydrogel. The gel was stained by BODIPY FL phallacidin solution.

## 6.2.2 Mechanical test

It was reported that the viability of the stem cell can be affected by many impacts. The physical interactions between ECM and cell is a very important aspect in regards to the effect towards cell viability[117] .It was shown by the previous research that the mechanical characteristics of matrix

could largely affect cell regeneration and differentiation [118]. In this project, the mechanical property of SWNT/Gelatin-APTS-$Fe_3O_4$ magnetic hydrogel was determined through stress-strain test. The deformation percent of hydrogel in the compression test was 50%. The result in figure 23 revealed that maximum stress of hydrogel is 34.8 kpa and the Young's modulus is 219kpa.

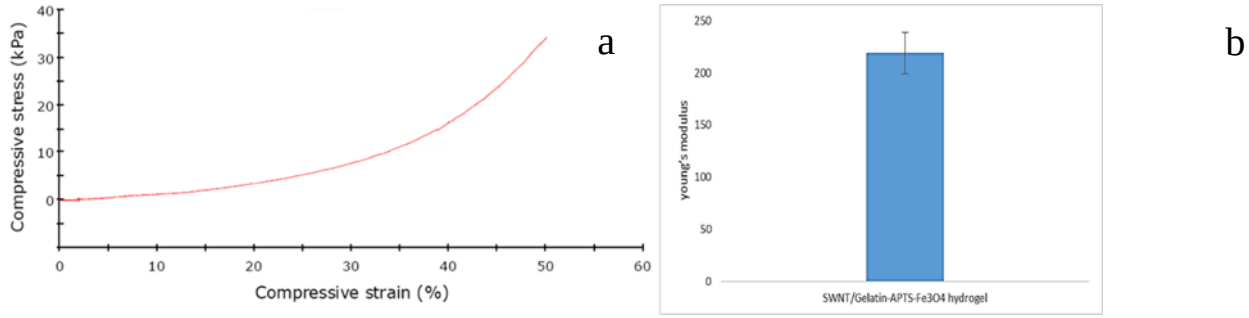


Figure 23 Representative stress–strain curve(a) and young's modulus(b) of SWNT/Gelatin-APTS-Fe3O4 magnetic hydrogel subjected to uniaxial compression testing (n=3).

### 6.2.3 The cell morphology of BMSC cells incubated with magnetic hydrogel

CLSM was employed to observe the cell morphology of BMSC cells incubated with magnetic hydrogel. As shown in Figure 24, in can be observed that the BMSC cells spread and migrate extensively after 24hs incubation with APTS-$Fe_3O_4$ magnetic hydrogel. The cytoplasm of BMSC cells exhibited silk like shape, and the nuclei were in a normal shape, suggesting that the magnetic hydrogel can provide good support for BMSC cell growth. The magnetic nanoparticles aggregation (as pointed by yellow arrow) can been seen clearly in the bright field confocal images of BMSC cells incubated with APTS-$Fe_3O_4$ magnetic hydrogel for 24hs (Figure 25)

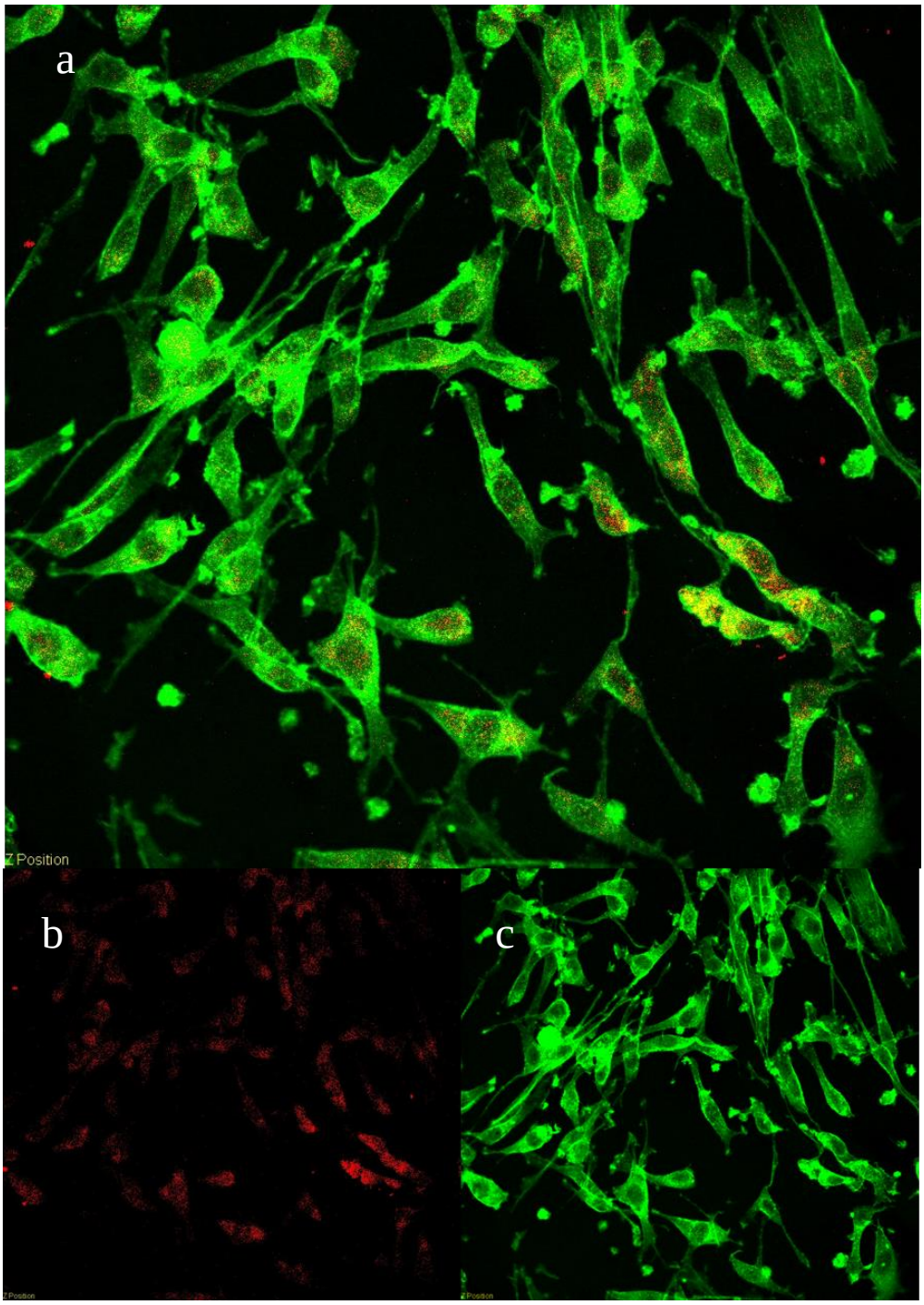


Figure 19 CLSM image of BMSC cells incubated with APTS-$Fe_3O_4$ hydrogel for 24hs. The green area displayed in figure c is the excited fluorescence of cytoplasm, the red area displayed in figure b is the excited fluorescence of nuclei. Figure a is the merge image of these two channels.

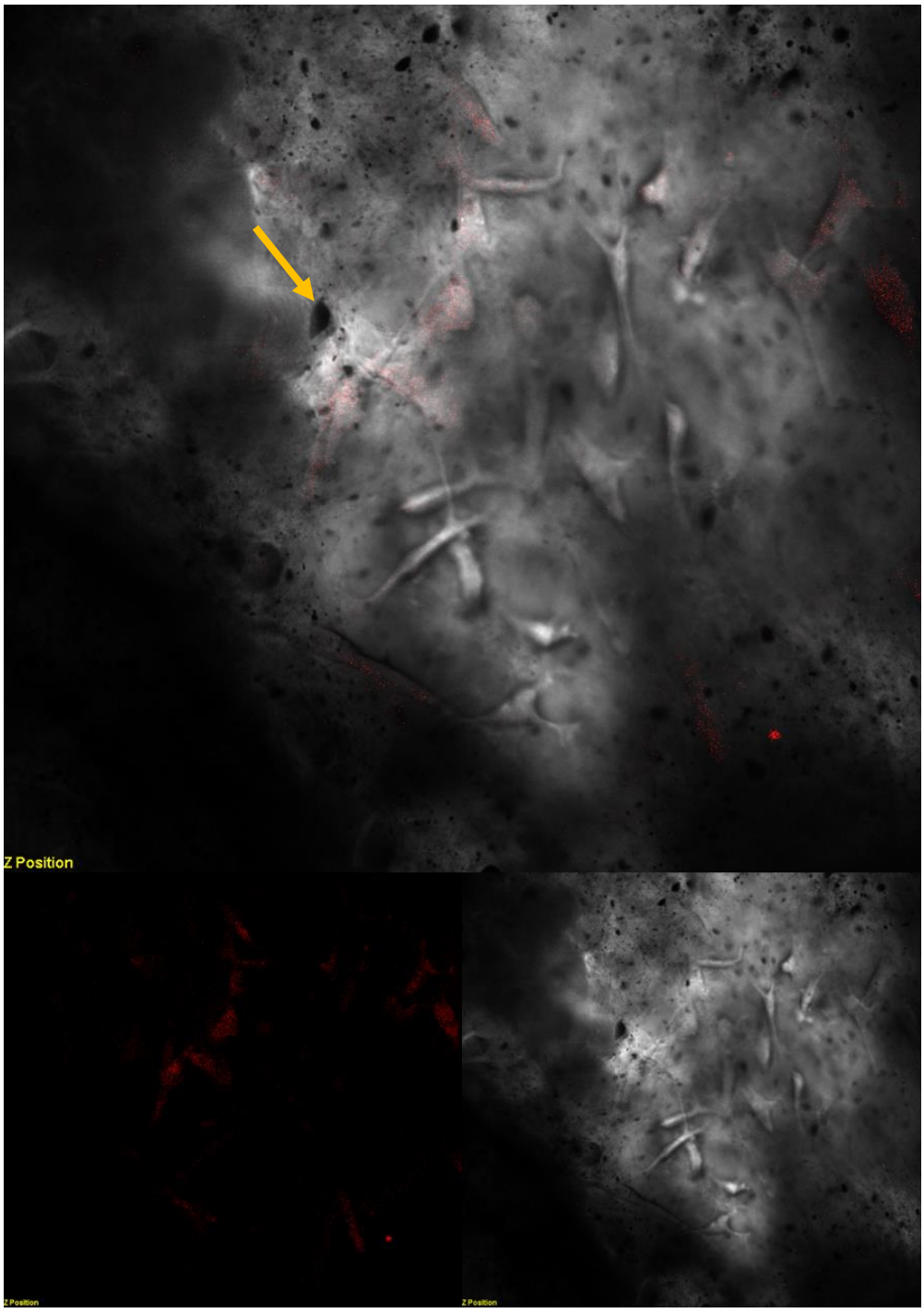


Figure 25 The bright field confocal images of BMSC cells incubated with APTS-$Fe_3O_4$ magnetic hydrogel for 24hs. The BMSC cells were incubated with APTS-$Fe_3O_4$ magnetic hydrogel for 24hs. The black dots shown in the image (as pointed out by yellow arrow) are APTS-$Fe_3O_4$ magnetic nanoparticles.

## 6.2.4 Cell viability

The cell viability of BMSC cells after incubated with SWNT/Gelatin-APTS-Fe3O4 magnetic hydrogel was determined by MTT assay. As exhibited in Figure 26, the viability of BMSC cells is 69% after 24hs incubation with SWNT/Gelatin-APTS-Fe3O4 magnetic hydrogel, the cell viability is 71% after 48hs incubation. This result agrees with the cell morphology test and also shows that the SWNT/Gelatin-APTS-Fe3O4 magnetic hydrogel will not affect the cell viability of BMSC cells, the hydrogel even provide a good support to cell growth.

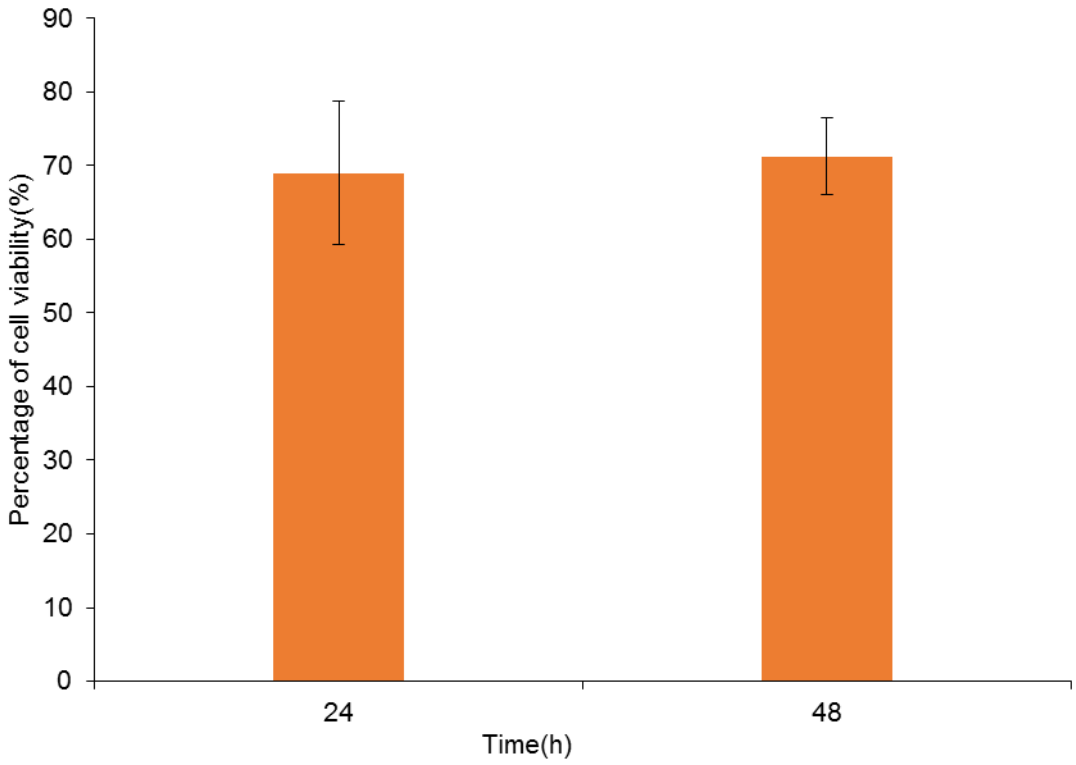


Figure 26 In vitro cytotoxicity of magnetic hydrogel on BMSC cells. The results are presented as mean values of three replications and standard deviation.

## 6.3 Summary

APTS-coated $Fe_3O_4$ magnetic hydrogel was successfully synthesized in this work. SEM images displayed the regularly distributed pores in the cross section of APTS- $Fe_3O_4$ hydrogel, which can provide much space for BMSC cell to grow and exhibit potential to carry drugs. The CLSM results show that cell morphology of BMSC cells was not affected by the hydrogel, in the contrast, the cell cytoplasm stretched very well. The result of MTT test also exhibits high cell viability after incubated with hydrogel. It is indicated by both CLSM results and MTT test results that the hydrogel can offer good support to the growth of BMSC cells.

# Chapter 7 Biocompatible SWNT/Gelatin-F127-cysteamine hydrogel for tissue engineering

## 7.1 Materials and Methods

### 7.1.1 Materials

Acryloyl chloride, N-methylpyrrolidone(NMP) were purchased from JenKem Technology USA Inc. (Allen, TX, US). Dialysis membrane (cut-off=7 kDa MWCO). Pluronic F-127, Gelatine, Dichloromethane, Diethyl ether, Cysteamine, Sodium sulfate and Glutaraldehyde were purchased from ACROS (New Jersey,USA). Pristine single-walled carbon nanotubes (Timesnano, prepared by chemical vapor deposition method, 90 wt % pure SWNTs, 1-2 nm in diameter and several micrometers in length) were used without further purification. Adipose-derived Stem Cells (ADSC) cells were purchased from ATCC.

### 7.1.2 Synthesis of F-127 DA

The typical synthesis was based on a previous study with modification and the protocol was describe as below [119]. 18g F-127 was dissolved in 30ml dichloromethane in ice bath. Acryloyl chloride was then carefully added to the solution for 25 times with 20ul for each time (500ul in all). Another

500ul of acryloyl chloride was carefully added with same method after 30min.11ml of acryloyl chloride was then directly added. After 24hs stirring, the mixture was then dialyzed against distilled water for 2 days. The final product was obtained by lyophilization and rate of yield was 88 %.

The chemical structure was next characterized by 1H NMR analysis. 1H-NMR spectra were recorded using a Bruker Avance 300 NMR spectrometer (300 MHz) with d6-DMSO as the solvent.

### 7.1.3 Synthesis of F-127 CT

The synthesis of F-127 CT was prepared based on a previous study with modification [120]. Briefly, 20g F127 DA and 15.18g cysteamine was dissolved in 100ml N-methylpyrrolidone(NMP) in nitrogen gas. The pH value of the solution was adjusted to 8 through addition of 2mol/l NaOH, following by 24hs stirring. The mixture was next dissolved in dichloromethane after rotary evaporate, then the solution was extracted by separating funnel after the addition of water. Certain amount of sodium sulfate was added to the solution and reserved for 24hs to remove water. The product was then purified by precipitation in largely excess of diethyl ether for three times. The white powder was dried in high vacuum for 24 h and the rate of yield was 92 %. The chemical structure was next characterized by 1H NMR analysis. 1H-NMR spectra were recorded using a Bruker Avance 300 NMR spectrometer (300 MHz) with d6-DMSO as the solvent.

### 7.1.4 Preparation of SWNT solution

The SWNT has attracted lots of attention due to its unique physicochemical characteristics. However some drawback has hindered its application in many arrears. One of the main disadvantages of SWNT is the poor stability and unevenly distribution in solution. F-127 is good surfactant in which SWNT could form a homogenous solution and remain stable. In this study,

240mg SWNT was added into 10ml 2% F-127 solution, after 2h s of sonication, the SWNT can distribute evenly in F-127 and form a black homogenous solution.

### 7.1.5 Preparation of SWNT based Gelatin-F-127 CT hydrogel

1ml F-127 CT was dissolved in 7.4 PBS buffer solution for 24hs in ice bath. 20ul 5% gelatin aqueous solution was next added into F-127 solution followed by 1min strong vortex stirring. Then, 20ul SWNT F-127 solution was added to the mixture followed by 10mins ultrasonic treatment. 90ul glutaraldehyde was next added to form hydrogel. The hydrogel was then washed by 7.4 PBS buffer solution for three times and then immersed in 7.4 PBS buffer solution for 24hs to remove excessive glutaraldehyde.

### 7.1.6 Determination of F-127DA and F-127CT

The chemical structure of F-127DA and F-127CT were characterized by $^{1}$H NMR analysis. d-DMSO was used as solvent. $^{1}$H NMR measurements were examined on a Bruker (500 MHz) NMR instrument.

### 7.1.7 Hydrogel morphology test

After cryosection, CLSM was carried out to explore the morphology of the SWNT/Gelatin-F127CT hydrogel. Firstly, hydrogel was immersed into 7.4 PBS buffer solution and was reserved for 24hs. The hydrogel was then fixed in cryomold using an O.C.T. compound. O.C.T. compound was next transferred to -80℃ freezer when it turn to solid phase in -20℃ cryomold. Next, hydrogel was transferred to cryostat from cryomold, hydrogel slides were then collected.

### 7.1.8 Swelling test

The freeze-dried SWNT/Gelatin-F127CT hydrogel was first weighted and then added into phosphate buffer solution buffer solution (pH=7.4). The hydrogel was taken out after predetermined time and the weight of hydrogel was written down. The SWNT-Gelatin-F127CT hydrogel was then immersed into PBS solution. The procedures mentioned above were carried out until the weight of hydrogel keep the same. Next the amount of the uptake of PBS solution was calculated as:

Water (%) = $(Wt - W_0)/W_0 \times 100$ (1)

Where $W_0$ represents the weight of the dried hydrogel and Wt represents the weight of hydrogels recorded each time.

### 7.1.9 Mechanical test of SWNT-Gelatin-F127CT hydrogel

The TA.XT2i Texture Analyzer (Texture Technologies Corp.) was used to explore the mechanical property of SWNT-Gelatin-F127CT hydrogel. The samples were prepared by the methods described below. Three cylinder shaped hydrogels with the diameter of 5mm and the height of 3mm were prepared by cutting blade. The parameter of compression test was set as below: the range of compression: 2mm and the speed of compression: 0.5mm/second. The mechanical property of hydrogel was gained form Analyzer software. All of tests were conducted in 28C (room temperature).

### 7.1.10 Rheological test

Rheological test of SWNT-Gelatin-F127CT hydrogel was conducted with an AR 2000 advanced rheometer (TA Instruments). In the oscillation procedure, 20mm 1° steel cone was used and the gap

was 52.00 micro meters. Compression distance was set to 119.0 micro meters, compression velocity was 3000.0 micrometer/s and shear rate factor was set to 57.29. Approximate sample volume was 40ul. The test was conducted for 6 min with a constant frequency (1Hz). The storage modulus (G'), the loss modulus (G") were obtained.

### 7.1.11 Hydrogel for cell culture

The SWNT-Gelatin-F127CT hydrogel applied for cell test was prepared by the following method: 100ul hydrogel precursor was added onto a piece of glass cover slip, then another glass cover slip was used to cover it. After successfully gelation, two cover slips were removed and the hydrogel was soaked in 7.4 PBS buffer for 24hs. Then, 7.4 PBS buffer was utilized to rinse hydrogel for three times. Next, the hydrogel was placed in bio-safety hood and irradiated by UV light for 1 hour to sterilize the hydrogel. The SWNT-Gelatin-F127CT hydrogel was next added into culture dish with agarose gel attached to the bottom.

### 7.1.12 Cell morphology test

After 24 h and 48h incubation with SWNT-Gelatin-F127CT hydrogel in 7.4 PBS buffer (0.1 M), the cell morphology of ADSC cells was explored by confocal laser scanning microscopy (CLSM). ADSC cells were cultured on the SWNT-Gelatin-F127CT hydrogel with the cell concentration of 2 x 105 cells/dish for predetermined time. PBS buffer was next used to wash the hydrogel-laden cells for three times. The cells were then fixed by immersing in 4 % paraformaldehyde PBS solution for 15min, hydrogel-laden cells were then rinsed with PBS buffer for three times. Cell morphology of ADSC cells were finally observed through CLSM after fixation on glass slide with cover slip.

## 7.2 Results and Discussions

### 7.2.1 The characterization of F-127DA and F-127CT

The chemical structures of F-127DA and F-127CT were characterized by $^{1}H$ NMR analysis. As shown in Figure 27, the peaks at 1.02 ppm, 3.32 ppm and 3.41 ppm are attributed to the typical proton peaks of methyl group, methine group and methylene group from PPG respectively. In the meantime, the peak at 3.61 is assigned to PEG chain protons. Moreover, the peak at 4.24 is assigned to proton a, the peaks from 5.92 to 6.39 are assigned to $H_b^1$, $H_b^2$ and $H_c$ from the double bonds. As shown in Figure 28, the peaks at 1.05 ppm is attributed to PPG methyl group, the peaks at 3.33 ppm, 3.43 ppm and 3.64 ppm are assigned to methine group, methylene group from PPG and PEG chain protons respectively. The peak at 2.64 is assigned to proton a. The peak at 4.15 is assigned to proton b.

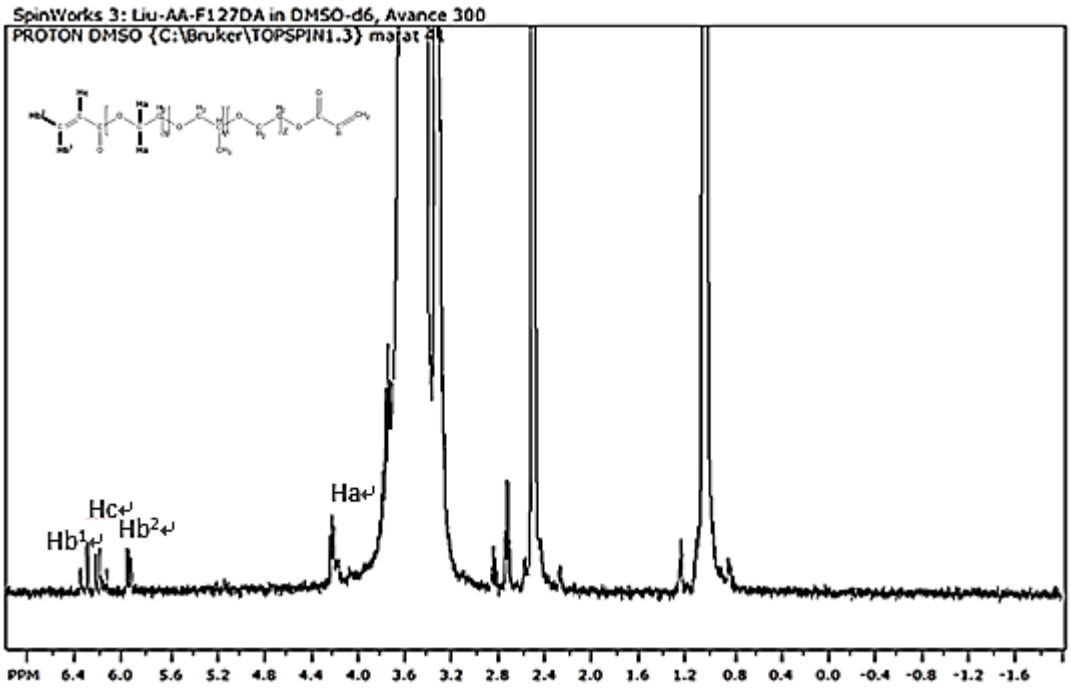


Figure 27 1H NMR of F-127 DA in dimethylsulfoxide-d6 (DMSO-d6)

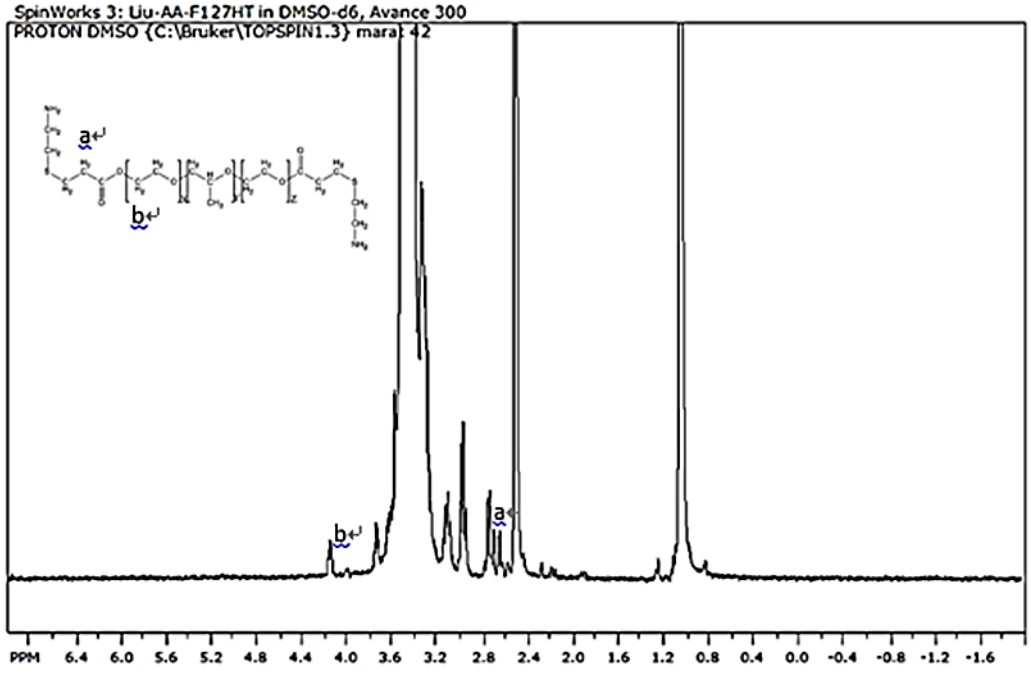


Figure 28 1H NMR of F-127 CT in dimethylsulfoxide-d6 (DMSO-d6)

## 7.2.2 Hydrogel morphology test

The morphology of SWNT-Gelatin-F127CT hydrogel was visualized by CLSM after cryosection. As can be seen in Figure 29, the cryosection image of SWNT-Gelatin-F127CT hydrogel wasexhibited clearly. After being immersed in 7.4 PBS for 24h. The pore size of hydrogel seen from the image varied between 100um~400um.

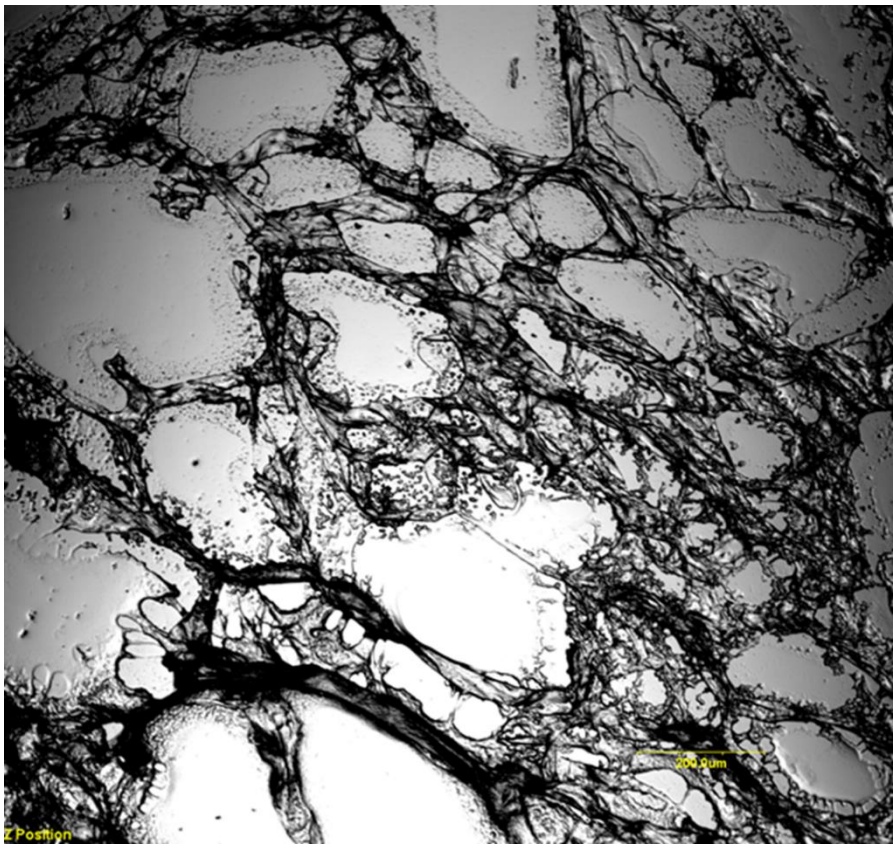


Figure 20 Cryosection images (The bright field confocal images) of SWNT-Gelatin-F127CT hydrogel.

## 7.2.3 Rheology test

The variation of elasticity and viscosity of a strong hydrogel and weak hydrogel could be affected by the storage modulus (G') and loss modulus (G") [121]. The storage modulus and loss modulus of SWNT-Gelatin-F127CT hydrogel were tested by rheology meter in this study. It can be seen from Figure 30 that both storage modulus and loss modulus were very low at the beginning, both the storage modulus and loss modulus increase with test time. The value of storage modulus became higher than the value of loss modulus after 50s and the difference between them was more and more obvious when test time increases, indicating the formation of SWNT-Gelatin-F127CT hydrogel.

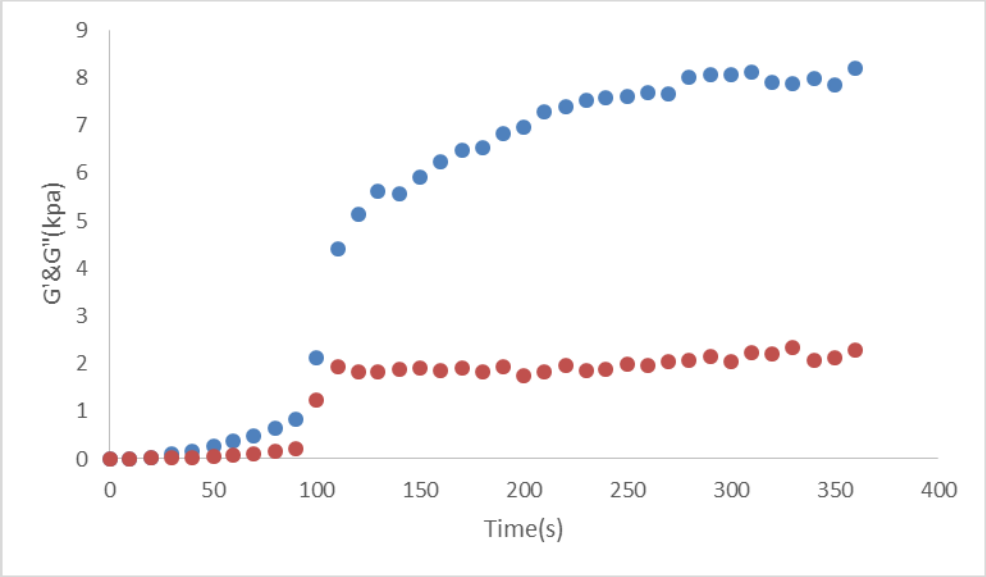


Figure 30 rheological properties of SWNT-Gelatin-F127CT hydrogel, the blue dots represent storage modulus and the red dots represent loss modulus.

### 7.2.4 The cell morphology of ADSC cells incubated with SWNT-Gelatin-F127CT hydrogel

The CLSM was employed to observe the cell morphology of ADSC cells incubated with SWNT-Gelatin-F127CT hydrogel. As shown in Figure 31, it can be observed that the ADSC cells spread and migrate extensively after 24hs and 48hs incubation with hydrogel. The cytoplasm of ADSC cells exhibited silk like shape, which reveals that the SWNT-Gelatin-F127CT hydrogel can provide good support for ADSC cell growth. The SWNT aggregates (as pointed by yellow arrow) can been seen clearly in the bright field confocal images of ADSC cells incubated with hydrogel for 48hs (Figure 32)

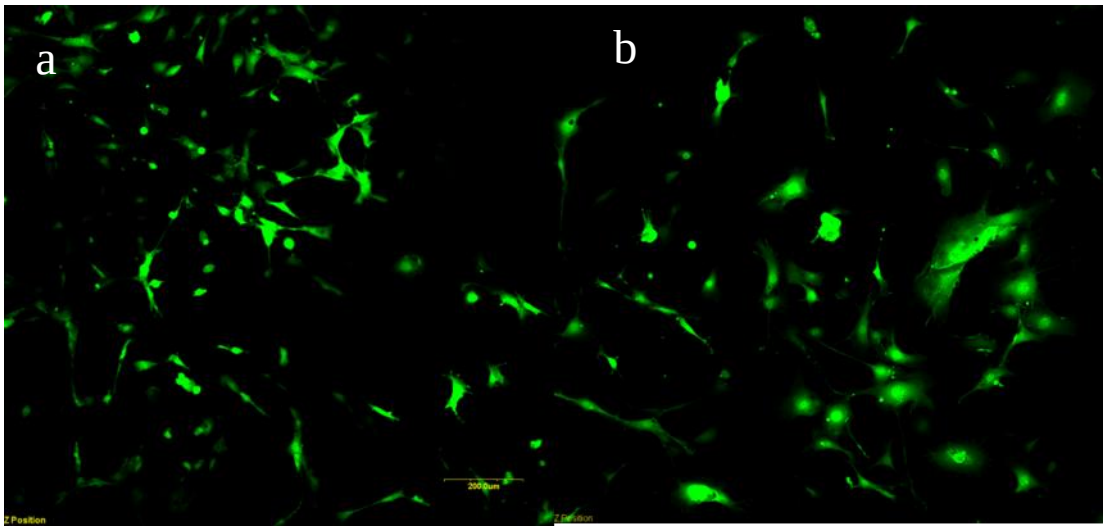


Figure 31 CLSM image of ADSC cells incubated with SWNT-Gelatin-F127CT hydrogel for 24hs(a) and 48hs(b).

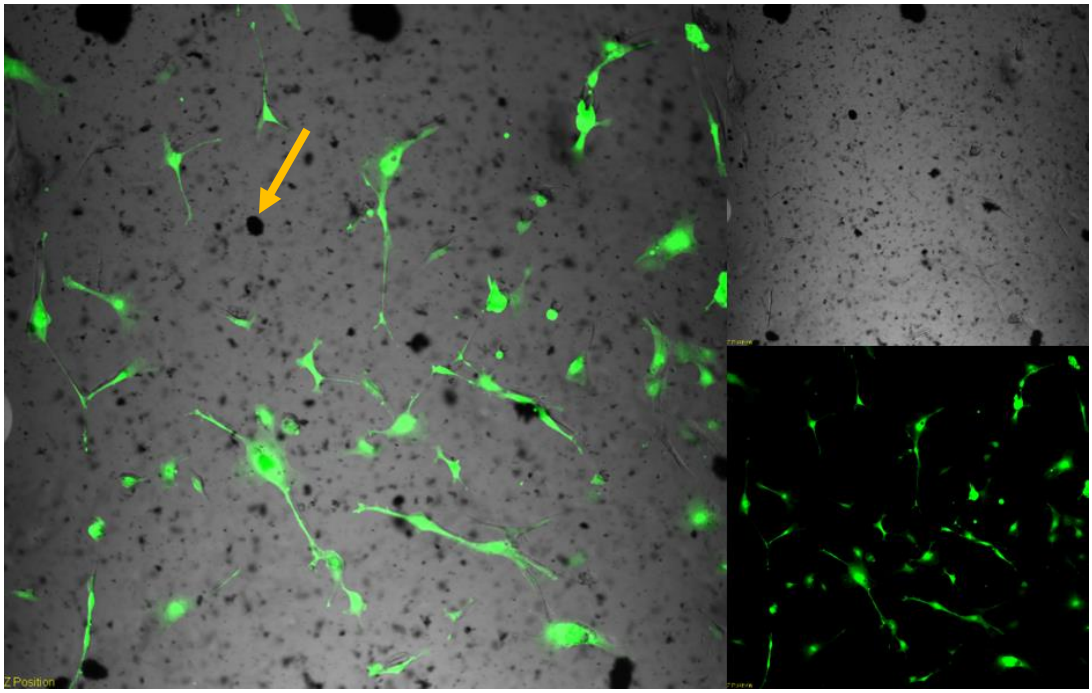

Figure 32 The bright field confocal images of ADSC cells incubated with SWNT-Gelatin-F127CT hydrogel for 48hs. The ADSC cells were incubated with SWNT-Gelatin-F127CT hydrogel for 48hs. The black dots shown in the image (as pointed out by yellow arrow) are aggregates of SWNT.

## 7.2.5 Swelling test

One vital characteristic of hydrogels is that they could absorb certain amount of water in response to the outer irritation. The swelling ability plays a crucial role in cell grows. When cells are incubated with hydrogel, the growth of cell is highly affected by the swelling ability of hydrogel: the higher the swelling capacity, the larger the area to which nutrients will spread, and the better the cell will grow. The swelling ability of hydrogel can be explored through the swelling ratio (the weight ratio between the water that has been absorbed by hydrogel in predetermined time point and the freeze-dried hydrogel). As shown in Figure 33, the swelling ratio of SWNT-Gelatin-F127CT hydrogel is 10 after 6 hs then can reach to 15 after 24hs, which is very outstanding and remain stable afterwards. The excellent swelling ability is one significant reason for its promising cell culture results.

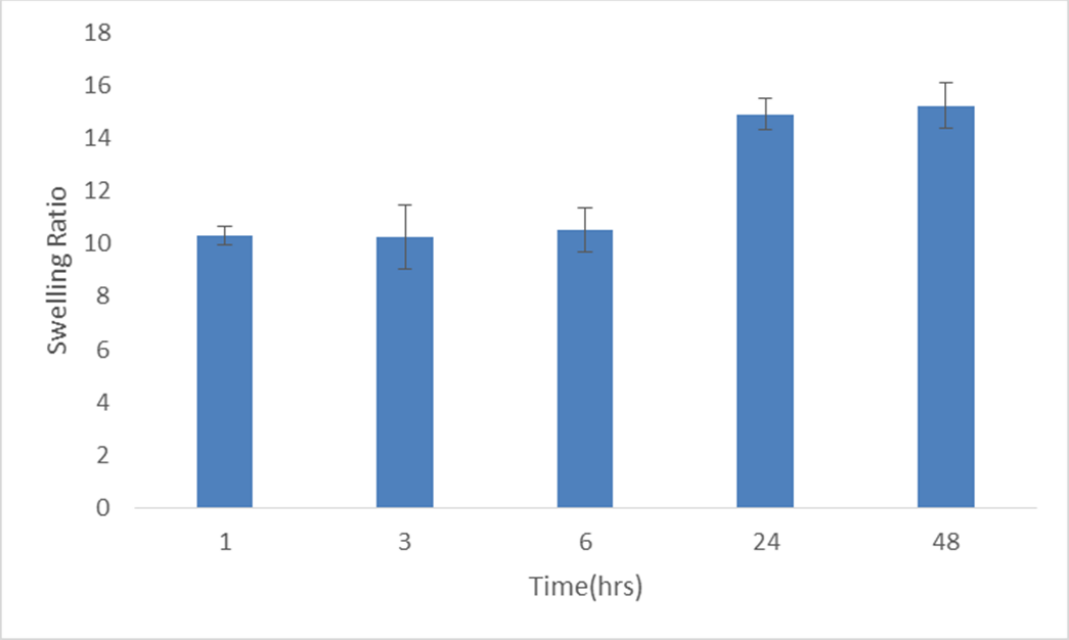


Figure 33 Swelling ratio of SWNT-Gelatin-F127CT hydrogel (n=3).

### 7.2.6 Stress-strain test

It has been reported that the differentiation and regeneration of cells could be influenced by the mechanical property of local matrix to a large extent[118]. The stress-strain test was conducted in this study to explore the mechanical property of SWNT-Gelatin-F127CT hydrogel. As can be seen in Figure 34, maximum stress is 14kpa which is similar to that of human tissue and the Young's modulus is 60. The mechanical test results show that the SWNT-Gelatin-F127CT hydrogel is very promising for application in later tissue engineering.

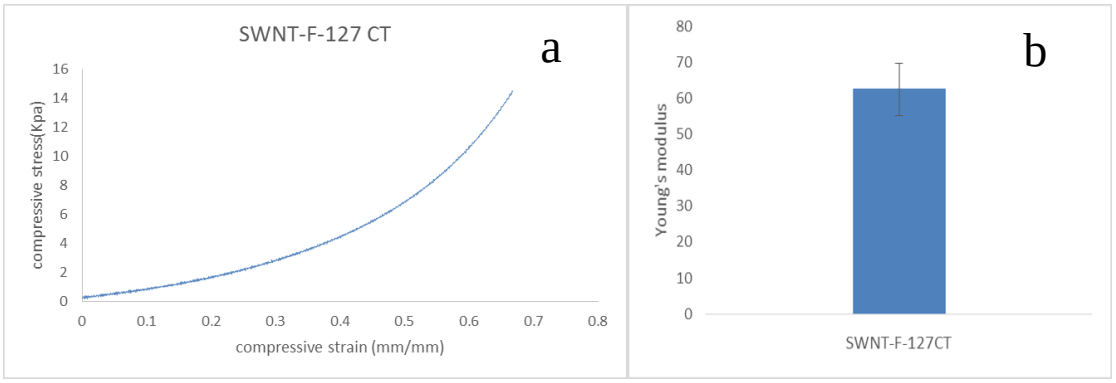


Figure 34 Representative stress–strain curve(a) and young's modulus(b) of SWNT-Gelatin-F127CT hydrogels subjected to uniaxial compression testing (n=3).

## 7.3 Summery

In this study, SWNT based Gelatin-F-127-cysteamine biocompatible hydrogel was successful developed, the SWNT in which is very stable and well distributed due to the existence of F-127. The successfully synthesis of F-127DA and F127CT was verified by FTIR and NMR. The cell morphology of ALSC was determined by confocal laser scanning microscopy (CLSM) and the results exhibited the good biocompatibility of this hydrogel. The excellent swelling ability of hydrogel was tested and the mechanical property of hydrogel was also explored. For the best of our

knowledge, this is the first time that SWNT, gelatin, cysteamine and F-127 were combined together and formed a biocompatible hydrogel, which has shown very promising potential in biomedical applications.

# 8 Conclusion

This thesis reports four SWNT-based projects on tumor therapy. In project one, a pH-sensitive poly(ethylene glycol)-doxorubicin(PEG-DOX)@SWNT drug release system was developed and the delivery of cancer drugs (DOX) from PEG-DOX@SWNT micelles was improved through exposure to NIR. In project two, a thermo-sensitive Gelatin/SWNT-APTS-$NH_2$ hydrogel was prepared and further proved to have the potential to be applied in the thermal treatment (through the exposure to NIR) towards cancer. In project three, a SWNT-based magnetic hydrogel was successfully prepared. It integrated the outstanding properties of carbon nanotubes and magnetic nanoparticles. The hydrogel can be used as a scaffold for BMSC cell growth and be applied in cardiac tissue engineering and magnetism based detecting test. In project four, a novel SWNT-Gelatin-F-127-cysteamine hydrogel was prepared. The hydrogel has high swelling capacity, good mechanical properties, therefore can be used as a scaffold for ADSC cell growth. The SWNT-Gelatin-F-127-cysteamine hydrogel prepared in this research can be further utilized in skin tissue regeneration studies.

# 9 Acknowledgement:

Foremost, I wish to express my sincere thanks to my advisor Dr. Wen Zhong, Department of Textile Science, and my co-advisor Dr. Malcolm Xing, Department of Mechanical engineering. Thanks for their professional, valuable and sincere instruction and encouragement extended to me, their guidance helped me in all phases of research and writing of this thesis.

Also, special acknowledgements are come to the rest of my thesis committee Dr. Alex C.-T. Ko, National Research Council Canada and Dr. Jiming Kong, Department of Human Anatomy and Cell Science, for their insightful comments and expert assist.

I also thank NSERC Discovery Grant and NSERC RTI Grant, and Manitoba Children's Foundation for their support.

Last but not the least, I would like to thanks my parent for their consistent encouragement and support.

Back Matter

# Bibliography


1. Iijima, S., *HELICAL MICROTUBULES OF GRAPHITIC CARBON.* NATURE, 1991. **354**(6348): p. 56-58.
2. P, H., Z. C, and X. C, *Preparation and characterization of near-infrared region absorption enhancer carbon nanotubes hybridmaterials.* Nano Biomed Eng, 2010(2): p. 225-230.
3. P, H., Z. C, and X. C, *Preparation and characterization of near-infrared region absorption enhancer carbon nanotubes hybridmaterials.* Nano Biomed Eng, 2010. **2**(4): p. 225-230.
4. Foldvari, M. and M. Bagonluri, *Carbon nanotubes as functional excipients for nanomedicines: II. Drug delivery and biocompatibility issues.* Nanomedicine-Nanotechnology Biology and Medicine, 2008. **4**(3): p. 183-200.
5. Liu, Z., et al., *Carbon Nanotubes in Biology and Medicine: In vitro and in vivo Detection, Imaging and Drug Delivery.* Nano Research, 2009. **2**(2): p. 85-120.
6. Joensuu, H., *Systemic chemotherapy for cancer: from weapon to treatment.* Lancet Oncology, 2008. **9**(3): p. 304-304.
7. Fornari, F.A., et al., *INTERFERENCE BY DOXORUBICIN WITH DNA UNWINDING IN MCF-7 BREAST-TUMOR CELLS.* Molecular Pharmacology, 1994. **45**(4): p. 649-656.
8. Momparler, R.L., et al., *EFFECT OF ADRIAMYCIN ON DNA, RNA, AND PROTEIN-SYNTHESIS IN CELL-FREE SYSTEMS AND INTACT-CELLS.* Cancer Research, 1976. **36**(8): p. 2891-2895.
9. L.P, O.B.P., *DOXIL Product Information.* 2007.
10. Weissleder, R., *A clearer vision for in vivo imaging.* Nature Biotechnology, 2001. **19**(4): p. 316-317.
11. Simpson, C.R., et al., *Near-infrared optical properties of ex vivo human skin and subcutaneous tissues measured using the Monte Carlo inversion technique.* Physics in Medicine and Biology, 1998. **43**(9): p. 2465-2478.
12. Ntziachristos, V., et al., *Looking and listening to light: the evolution of whole-body photonic imaging.* Nature Biotechnology, 2005. **23**(3): p. 313-320.
13. Vaupel, P., F. Kallinowski, and P. Okunieff, *BLOOD-FLOW, OXYGEN AND NUTRIENT SUPPLY, AND METABOLIC MICROENVIRONMENT OF HUMAN-TUMORS - A REVIEW.* Cancer Research, 1989. **49**(23): p. 6449-6465.
14. Tannock, I.F. and D. Rotin, *ACID PH IN TUMORS AND ITS POTENTIAL FOR THERAPEUTIC EXPLOITATION.* Cancer Research, 1989. **49**(16): p. 4373-4384.

15. McCarty, M.F. and J. Whitaker, *Manipulating Tumor Acidification as a Cancer Treatment Strategy.* Alternative Medicine Review, 2010. **15**(3): p. 264-272.
16. Wichterle, O. and D. Lim, *HYDROPHILIC GELS FOR BIOLOGICAL USE.* NATURE, 1960. **185**(4706): p. 117-118.
17. Kam, N.W.S. and H.J. Dai, *Carbon nanotubes as intracellular protein transporters: Generality and biological functionality.* Journal of the American Chemical Society, 2005. **127**(16): p. 6021-6026.
18. Pantarotto, D., et al., *Functionalized carbon nanotubes for plasmid DNA gene delivery.* Angewandte Chemie-International Edition, 2004. **43**(39): p. 5242-5246.
19. Kostarelos, K., et al., *Cellular uptake of functionalized carbon nanotubes is independent of functional group and cell type.* Nature Nanotechnology, 2007. **2**(2): p. 108-113.
20. Y, L., W. DC, and Z. WD, *Polyethylenimine-grafted multiwalled carbon nanotbue for secure noncovalent immobilization and efficient delivery of DNA.* Angew Chem Int Ed., 2005. **44**(30): p. 4782–4785.
21. NW, K., L. Z, and D.H. J, *Functionalization of carbon nanotbues via cleavable disulfide bonds for efficient intracelluar delivery of siRNA and potent gene silencing.* Am Chem Soc., 2005. **127**(36): p. 12492–12493.
22. Pankhurst, Q.A., et al., *Applications of magnetic nanoparticles in biomedicine.* Journal of Physics D-Applied Physics, 2003. **36**(13): p. R167-R181.
23. Gupta, A.K. and M. Gupta, *Synthesis and surface engineering of iron oxide nanoparticles for biomedical applications.* Biomaterials, 2005. **26**(18): p. 3995-4021.
24. Sun, C., J.S.H. Lee, and M. Zhang, *Magnetic nanoparticles in MR imaging and drug delivery.* Advanced Drug Delivery Reviews, 2008. **60**(11): p. 1252-1265.
25. Sun, S., et al., *Affinity adsorption and separation behaviors of avidin on biofunctional magnetic nanoparticles binding to iminobiotin.* Colloids and Surfaces B-Biointerfaces, 2011. **88**(1): p. 246-253.
26. Horie, M., et al., *Dispersant affects the cellular influences of single-wall carbon nanotube: the role of CNT as carrier of dispersants.* Toxicology Mechanisms and Methods, 2013. **23**(5): p. 315-322.
27. Alpatova, A.L., et al., *Single-walled carbon nanotubes dispersed in aqueous media via non-covalent functionalization: Effect of dispersant on the stability, cytotoxicity, and epigenetic toxicity of nanotube suspensions.* Water Research, 2010. **44**(2): p. 505-520.
28. Schmolka, I.R., *ARTIFICIAL SKIN .1. PREPARATION AND PROPERTIES OF PLURONIC F-127 GELS FOR TREATMENT OF BURNS.* Journal of Biomedical Materials Research, 1972. **6**(6): p. 571-&.
29. Bardi, G., et al., *Adipocytes differentiation in the presence of Pluronic F127-coated carbon nanotubes.* Nanomedicine-Nanotechnology Biology and Medicine, 2009. **5**(4): p. 378-381.
30. Fukumori, Y. and H. Ichikawa, *Nanoparticles for cancer therapy and diagnosis.* Advanced Powder Technology, 2006. **17**(1): p. 1-28.
31. Vasir, J.K. and V. Labhasetwar, *Biodegradable nanoparticles for cytosolic delivery of therapeutics.* Advanced Drug Delivery Reviews, 2007. **59**(8): p. 718-728.
32. Faraji, A.H. and P. Wipf, *Nanoparticles in cellular drug delivery.* Bioorganic & Medicinal Chemistry, 2009. **17**(8): p. 2950-2962.
33. Vashist, S.K., et al., *Delivery of drugs and biomolecules using carbon nanotubes.* Carbon, 2011. **49**(13): p. 4077-4097.

34. D, C., Z. H, and S. J, *Effects of CdSe/ZnS quantum dots covered multi-walled carbon nanotubes on murine embryonic stem cells.* Nano Biomed Eng, 2010. **2**(4): p. 236-244.
35. Panhuis, M.I.H., *Vaccine delivery by carbon nanotubes.* Chemistry & Biology, 2003. **10**(10): p. 897-898.
36. W., X.Z. and Z.Z. Z., *The application of carbon nanotubes in target drug delivery systems for cancer therapies.* Nanoscale Research Letters, 2011: p. 1-22.
37. Wang, J., *Electroanalysis.* 2005. **7**(7).
38. Sinha, N. and J.T.W. Yeow, *Carbon nanotubes for biomedical applications.* Ieee Transactions on Nanobioscience, 2005. **4**(2): p. 180-195.
39. Yang, Z., et al., *Pharmacological and toxicological target organelles and safe use of single-walled carbon nanotubes as drug carriers in treating Alzheimer disease.* Nanomedicine-Nanotechnology Biology and Medicine, 2010. **6**(3): p. 427-441.
40. NWS, K., W. JA, and D. HJ, *Proceedings of the national academy of sciences of the united states of America.* 2005. **102**: p. 11600－11605.
41. Leeuw, T.K., et al., *Single-walled carbon nanotubes in the intact organism: Near-IR imaging and biocompatibility studies in Drosophila.* NANO LETTERS, 2007. **7**(9): p. 2650-2654.
42. Liu, Z., et al., *Circulation and long-term fate of functionalized, biocompatible single-walled carbon nanotubes in mice probed by Raman spectroscopy.* Proceedings of the National Academy of Sciences of the United States of America, 2008. **105**(5): p. 1410-1415.
43. Bhirde, A.A., et al., *Targeted Killing of Cancer Cells in Vivo and in Vitro with EGF-Directed Carbon Nanotube-Based Drug Delivery.* Acs Nano, 2009. **3**(2): p. 307-316.
44. Zhang, X., et al., *Targeted delivery and controlled release of doxorubicin to cancer cells using modified single wall carbon nanotubes.* Biomaterials, 2009. **30**(30): p. 6041-6047.
45. Duong, H.M., et al., *A numerical study on the effective thermal conductivity of biological fluids containing single-walled carbon nanotubes.* International Journal of Heat and Mass Transfer, 2009. **52**(23-24): p. 5591-5597.
46. Pantarotto, D., et al., *Translocation of bioactive peptides across cell membranes by carbon nanotubes.* Chemical Communications, 2004(1): p. 16-17.
47. Kam, N.W.S., et al., *Nanotube molecular transporters: Internalization of carbon nanotube-protein conjugates into mammalian cells.* Journal of the American Chemical Society, 2004. **126**(22): p. 6850-6851.
48. K, A., Y. M, and M. T, *Carbon nanohorns as anticancer drug carriers.* Acta Pharmaceutica Sinica, 2008. **43**(10): p. 985-991.
49. Muralkami, T., et al., *Drug-loaded carbon nanohorns: Adsorption and release of dexamethasone in vitro.* Molecular Pharmaceutics, 2004. **1**(6): p. 399-405.
50. Shiba, K., M. Yudasaka, and S. Iijima, *Carbon nanohorns as a novel drug carrier.* Nihon rinsho. Japanese journal of clinical medicine, 2006. **64**(2): p. 239-46.
51. Foldvari, M. and M. Bagonluri, *Carbon nanotubes as functional excipients for nanomedicines: I. pharmaceutical properties.* Nanomedicine-Nanotechnology Biology and Medicine, 2008. **4**(3): p. 173-182.
52. Prato, M., K. Kostarelos, and A. Bianco, *Functionalized carbon nanotubes in drug design and discovery.* Accounts of Chemical Research, 2008. **41**(1): p. 60-68.
53. Z, h., T. W, and H. A, *Reactivity of the convex and concave surfaces of single-walled carbon nanotubes (SWNTs) towards addition reactions: dependence on the carbon-atom pyramidalization.* Chem Phys Chem, 2003. **4**: p. 93-97.

54. Liu, Z., et al., *Supramolecular chemistry on water-soluble carbon nanotubes for drug loading and delivery.* Acs Nano, 2007. **1**(1): p. 50-56.
55. Liu, Y., et al., *Polyethylenimine-grafted multiwalled carbon nanotubes for secure noncovalent immobilization and efficient delivery of DNA.* Angewandte Chemie-International Edition, 2005. **44**(30): p. 4782-4785.
56. Yinghuai, Z., et al., *Substituted carborane-appended water-soluble single-wall carbon nanotubes: New approach to boron neutron capture therapy drug delivery.* Journal of the American Chemical Society, 2005. **127**(27): p. 9875-9880.
57. Cheng, J., et al., *Reversible Accumulation of PEGylated Single-Walled Carbon Nanotubes in the Mammalian Nucleus.* Acs Nano, 2008. **2**(10): p. 2085-2094.
58. Magrez, A., et al., *Cellular toxicity of carbon-based nanomaterials.* NANO LETTERS, 2006. **6**(6): p. 1121-1125.
59. Murugesan, S., et al., *Blood compatible carbon nanotubes - Nano-based neoproteoglycans.* Langmuir, 2006. **22**(8): p. 3461-3463.
60. S, P., Y. HS, and K. D, *Rational design of amphiphilic polymers to make carbon nanotubes waterdispersible, anti-biofouling, and functionalizable.* Chem Commun, 2008. **25**: p. 2876.
61. Heister, E., et al., *Triple functionalisation of single-walled carbon nanotubes with doxorubicin, a monoclonal antibody, and a fluorescent marker for targeted cancer therapy.* Carbon, 2009. **47**(9): p. 2152-2160.
62. Liu, Z., et al., *Supramolecular Stacking of Doxorubicin on Carbon Nanotubes for In Vivo Cancer Therapy.* Angewandte Chemie-International Edition, 2009. **48**(41): p. 7668-7672.
63. Ali-Boucetta, H., et al., *Multiwalled carbon nanotube-doxorubicin supramolecular complexes for cancer therapeutics.* Chemical Communications, 2008(4): p. 459-461.
64. R, L., W. R, and Z. L, *Folate and iron difunctionalized multiwall carbon nanotubes as dualtargeted drug nanocarrier to cancer cells.* Carbon, 2011. **49**(5): p. 1797–1805.
65. Chen, Z., et al., *Adsorption behavior of epirubicin hydrochloride on carboxylated carbon nanotubes.* International Journal of Pharmaceutics, 2011. **405**(1-2): p. 153-161.
66. Meng, F., Z. Zhong, and J. Feijen, *Stimuli-Responsive Polymersomes for Programmed Drug Delivery.* Biomacromolecules, 2009. **10**(2): p. 197-209.
67. Martin, G.R. and R.K. Jain, *NONINVASIVE MEASUREMENT OF INTERSTITIAL PH PROFILES IN NORMAL AND NEOPLASTIC TISSUE USING FLUORESCENCE RATIO IMAGING MICROSCOPY.* Cancer Research, 1994. **54**(21): p. 5670-5674.
68. Engin, K., et al., *EXTRACELLULAR PH DISTRIBUTION IN HUMAN TUMORS.* International Journal of Hyperthermia, 1995. **11**(2): p. 211-216.
69. ZM, B., R. N, and B. P, *In vivo imaging of extracellular pH using H-1 MRSI.* Magnet Reson Med, 1999. **41**(4): p. 743—750.
70. Yan, E., et al., *Polymer/silica hybrid hollow nanospheres with pH-sensitive drug release in physiological and intracellular environments.* Chemical Communications, 2009(19): p. 2718-2720.
71. Schmaljohann, D., *Thermo- and pH-responsive polymers in drug delivery.* Advanced Drug Delivery Reviews, 2006. **58**(15): p. 1655-1670.
72. Hu, Y., et al., *Cytosolic delivery of membrane-impermeable molecules in dendritic cells using pH-Responsive core-shell nanoparticles.* NANO LETTERS, 2007. **7**(10): p. 3056-3064.

73. Yin, H., et al., *Physicochemical characteristics of pH-sensitive poly(L-Histidine)-b-poly (ethylene glycol)/poly(L-Lactide)-b-poly(ethylene glycol) mixed micelles.* Journal of Controlled Release, 2008. **126**(2): p. 130-138.
74. Sethuraman, V.A., K. Na, and Y.H. Bae, *pH-responsive sulfonamide/PEI system for tumor specific gene delivery: An in vitro study.* Biomacromolecules, 2006. **7**(1): p. 64-70.
75. K, P., S. WSW, and P. H., *Biodegradable Hydrogel For Drug Delivery.* Lancaster: Technomic, 1993.
76. Kamath, K.R. and K. Park, *BIODEGRADABLE HYDROGELS IN DRUG-DELIVERY.* Advanced Drug Delivery Reviews, 1993. **11**(1-2): p. 59-84.
77. Hoffman, A.S., *Hydrogels for biomedical applications.* Advanced Drug Delivery Reviews, 2002. **54**(1): p. 3-12.
78. Kashyap, N., N. Kumar, and M. Kumar, *Hydrogels for pharmaceutical and biomedical applications.* Critical Reviews in Therapeutic Drug Carrier Systems, 2005. **22**(2): p. 107-149.
79. AS, H., *Controlled Drug Delivery: Challenge and Strategies.* merican Chemical Society, 1997.
80. YH, B., *Controlled Drug Delivery: Challenge and Strategies.* American Chemical Society, 1997.
81. Kost, J. and R. Langer, *Responsive polymeric delivery systems.* Advanced Drug Delivery Reviews, 2001. **46**(1-3): p. 125-148.
82. ER, G., L. JC, and E. J, Pharm Biopharm, 2004. **58**: p. 409.
83. Corot, C., et al., *Recent advances in iron oxide nanocrystal technology for medical imaging.* Advanced Drug Delivery Reviews, 2006. **58**(14): p. 1471-1504.
84. Mornet, S., et al., *Magnetic nanoparticle design for medical diagnosis and therapy.* Journal of Materials Chemistry, 2004. **14**(14): p. 2161-2175.
85. Liu, S., et al., *NIR initiated and pH sensitive single-wall carbon nanotubes for doxorubicin intracellular delivery.* Journal of Materials Chemistry B, 2014: p. DOI: 10.1039/C3TB21362E.
86. Huan, M., et al., *In Vitro and In Vivo Antitumor Activity of a Novel pH-Activated Polymeric Drug Delivery System for Doxorubicin.* PloS one, 2012. **7**(9): p. e44116.
87. Yoo, H.S., E.A. Lee, and T.G. Park, *Doxorubicin-conjugated biodegradable polymeric micelles having acid-cleavable linkages.* Journal of Controlled Release, 2002. **82**(1): p. 17-27.
88. Ren, J., et al., *The targeted delivery of anticancer drugs to brain glioma by PEGylated oxidized multi-walled carbon nanotubes modified with angiopep-2.* Biomaterials, 2012. **33**(11): p. 3324-3333.
89. H, A.-B., et al., *Multiwalled carbon nanotube-doxorubicin supramolecular complexes for cancer therapeutics.* Chem Comm., 2008(4): p. 459–461.
90. Z, L., F. AC, and R. K, *Supermolecular stacking of doxorubicin on carbon nanotubes for in vivo cancer therapy.* Angew Chem Int Ed., 2009. **48**(41): p. 7668–7672.
91. Rihova, B., et al., *Synergistic Action of Doxorubicin Bound to the Polymeric Carrier Based on N-(2-Hydroxypropyl)methacrylamide Copolymers through an Amide or Hydrazone Bond.* Molecular Pharmaceutics, 2010. **7**(4): p. 1027-1040.
92. Wack, K.E., et al., *Sinusoidal ultrastructure evaluated during the revascularization of regenerating rat liver.* Hepatology, 2001. **33**(2): p. 363-378.

93. Pezacki, J.P., et al., *Chemical contrast for imaging living systems: molecular vibrations drive CARS microscopy.* Nature Chemical Biology, 2011. **7**(3): p. 137-145.
94. Etrych, T., et al., *New HPMA copolymers containing doxorubicin bound via pH-sensitive linkage: synthesis and preliminary in vitro and in vivo biological properties.* Journal of Controlled Release, 2001. **73**(1): p. 89-102.
95. Yang, X., et al., *Tumor-Targeting, pH-Responsive, and Stable Unimolecular Micelles as Drug Nanocarriers for Targeted Cancer Therapy.* Bioconjugate Chemistry, 2010. **21**(3): p. 496-504.
96. CC, L., et al., *Tumor-targeting, pHresponsive, and stable unimolecular micelles as drug nanocarriers for targeted cancer therapy.* Bioconjugate Chemistry, 2006. **17**(3): p. 496–504.
97. Aryal, S., et al., *Doxorubicin conjugated gold nanoparticles as water-soluble and pH-responsive anticancer drug nanocarriers.* Journal of Materials Chemistry, 2009. **19**(42): p. 7879-7884.
98. Prabaharan, M., et al., *Gold nanoparticles with a monolayer of doxorubicin-conjugated amphiphilic block copolymer for tumor-targeted drug delivery.* Biomaterials, 2009. **30**(30): p. 6065-6075.
99. Singh, K.V., et al., *Covalent functionalization of single walled carbon nanotubes with peptide nucleic acid: Nanocomponents for molecular level electronics.* Carbon, 2006. **44**(9): p. 1730-1739.
100. Huang, H., et al., *A new family of folate-decorated and carbon nanotube-mediated drug delivery system: Synthesis and drug delivery response.* Advanced Drug Delivery Reviews, 2011. **63**(14-15): p. 1332-1339.
101. Chiang, Y.-C., W.-H. Lin, and Y.-C. Chang, *The influence of treatment duration on multi-walled carbon nanotubes functionalized by H2SO4/HNO3 oxidation.* Applied Surface Science, 2011. **257**(6): p. 2401-2410.
102. Datsyuk, V., et al., *Chemical oxidation of multiwalled carbon nanotubes.* Carbon, 2008. **46**(6): p. 833-840.
103. Zhang, N.Y., J. Me, and V.K. Varadan, *Functionalization of carbon nanotubes by potassium permanganate assisted with phase transfer catalyst.* Smart Materials & Structures, 2002. **11**(6): p. 962-965.
104. Pirlot, C., et al., *Preparation and characterization of carbon nanotube/polyacrylonitrile composites.* Advanced Engineering Materials, 2002. **4**(3): p. 109-114.
105. Rofstad, E.K., et al., *Acidic extracellular pH promotes experimental metastasis of human melanoma cells in athymic nude mice.* Cancer Research, 2006. **66**(13): p. 6699-6707.
106. Watson, P., A.T. Jones, and D.J. Stephens, *Intracellular trafficking pathways and drug delivery: fluorescence imaging of living and fixed cells.* Advanced Drug Delivery Reviews, 2005. **57**(1): p. 43-61.
107. Kale, A.A. and V.P. Torchilin, *Design, synthesis, and characterization of pH-sensitive PEG-PE conjugates for stimuli-sensitive pharmaceutical nanocarriers: The effect of substitutes at the hydrazone linkage on the pH stability of PEG-PE conjugates.* Bioconjugate Chemistry, 2007. **18**(2): p. 363-370.
108. Kono, K., et al., *Preparation and cytotoxic activity of poly(ethylene glycol)-modified poly(amidoamine) dendrimers bearing adriamycin.* Biomaterials, 2008. **29**(11): p. 1664-1675.

109. Rodrigues, P.C.A., et al., *Acid-sensitive polyethylene glycol conjugates of doxorubicin: Preparation, in vitro efficacy and intracellular distribution.* Bioorganic & Medicinal Chemistry, 1999. **7**(11): p. 2517-2524.
110. Fujigaya, T., T. Morimoto, and N. Nakashima, *Isolated single-walled carbon nanotubes in a gel as a molecular reservoir and its application to controlled drug release triggered by near-IR laser irradiation.* Soft Matter, 2011. **7**(6): p. 2647-2652.
111. Wang, C., et al., *A chitosan-modified graphene nanogel for noninvasive controlled drug release.* Nanomedicine-Nanotechnology Biology and Medicine, 2013. **9**(7): p. 903-911.
112. Kim, H., et al., *Photothermally Triggered Cytosolic Drug Delivery via Endosome Disruption Using a Functionalized Reduced Graphene Oxide.* Acs Nano, 2013. **7**(8): p. 6735-6746.
113. Chen, J., et al., *Mechanical, rheological and release behaviors of a poloxamer 407/ poloxamer 188/carbopol 940 thermosensitive composite hydrogel.* Molecules (Basel, Switzerland), 2013. **18**(10): p. 12415-25.
114. Badruddoza, A.Z., K. Hidajat, and M.S. Uddin, *Synthesis and characterization of beta-cyclodextrin-conjugated magnetic nanoparticles and their uses as solid-phase artificial chaperones in refolding of carbonic anhydrase bovine.* J Colloid Interface Sci, 2010. **346**(2): p. 337-46.
115. Yamaura, M., et al., *Preparation and characterization of (3-aminopropyl) triethoxysilane-coated magnetite nanoparticles.* Journal of Magnetism and Magnetic Materials, 2004. **279**(2-3): p. 210-217.
116. Netto, C.G.C.M., et al., *Catalytic properties of thioredoxin immobilized on superparamagnetic nanoparticles.* Journal of Inorganic Biochemistry, 2011. **105**(5): p. 738-744.
117. Guilak, F., et al., *Control of Stem Cell Fate by Physical Interactions with the Extracellular Matrix.* Cell Stem Cell, 2009. **5**(1): p. 17-26.
118. Discher, D.E., P. Janmey, and Y.L. Wang, *Tissue cells feel and respond to the stiffness of their substrate.* Science, 2005. **310**(5751): p. 1139-1143.
119. Young, M., L and S. Seong, L, *Hydrogels of poly(ethylene glycol)-copoly(lactones) diacrylate macromers and/3-chitin.* Polymer, 1996. **38**: p. 2415-2420.
120. Cellesi, F., N. Tirelli, and J.A. Hubbell, *Materials for cell encapsulation via a new tandem approach combining reverse thermal gelation and covalent crosslinking.* Macromolecular Chemistry and Physics, 2002. **203**(10-11): p. 1466-1472.
121. Jones, D.S., A.D. Woolfson, and J. Djokic, *Texture profile analysis of bioadhesive polymeric semisolids: Mechanical characterization and investigation of interactions between formulation components.* Journal of Applied Polymer Science, 1996. **61**(12): p. 2229-2234.